Mon. Not. R. Astron. Soc. **358,** 503–520 (2005) doi:10.1111/j.1365-2966.2005.08855.x

Structure and kinematics of edge-on galaxy discs – V. The dynamics of stellar discs

M. Kregel,[1] P. C. van der Kruit[1]⋆ and K. C. Freeman[2]

[1]*Kapteyn Astronomical Institute, University of Groningen, PO Box 800, 9700AV Groningen, the Netherlands*
[2]*Research School for Astronomy and Astrophysics, Mount Stromlo Observatory, The Australian National University, Private Bag, Weston Creek, 2611 Canberra, Australia*

Accepted 2005 January 17. Received 2005 January 12; in original form 2004 June 10

ABSTRACT

In earlier papers in this series we determined the intrinsic stellar disc kinematics of 15 intermediate- to late-type edge-on spiral galaxies using a dynamical modelling technique. The sample covers a substantial range in maximum rotation velocity and deprojected face-on surface brightness, and contains seven spirals with either a boxy or peanut-shaped bulge. Here we discuss the structural, kinematical and dynamical properties. From the photometry we find that intrinsically more flattened discs tend to have a lower face-on central surface brightness and a larger dynamical mass-to-light ratio. This observation suggests that, at a constant maximum rotational velocity, lower surface brightness discs have smaller vertical stellar velocity dispersions.

Although the individual uncertainties are large, we find from the dynamical modelling that at least 12 discs are submaximal. The average disc contributes 53 ± 4 per cent to the observed rotation at 2.2 disc scalelengths (h_R), with a 1σ scatter of 15 per cent. This percentage becomes somewhat lower when effects of finite disc flattening and gravity by the dark halo and the gas are taken into account. Since boxy and peanut-shaped bulges are probably associated with bars, the result suggests that at $2.2\,h_R$ the submaximal nature of discs is independent of barredness. The possibility remains that very high surface brightness discs are maximal, as these discs are underrepresented in our sample. We confirm that the radial stellar disc velocity dispersion is related to the galaxy maximum rotational velocity. The scatter in this σ versus $v_{\rm max}$ relation appears to correlate with the disc flattening, face-on central surface brightness and dynamical mass-to-light ratio. Low surface brightness discs tend to be more flattened and have smaller stellar velocity dispersions. The findings are consistent with the observed correlation between disc flattening and dynamical mass-to-light ratio and can generally be reproduced by the simple collapse theory for disc galaxy formation. Finally, the disc mass Tully–Fisher relation is offset from the maximum-disc scaled stellar mass Tully–Fisher relation of the Ursa Major cluster. This offset, -0.3 dex in mass, is naturally explained if the discs of the Ursa Major cluster spirals are submaximal.

Key words: galaxies: fundamental parameters – galaxies: kinematics and dynamics – galaxies: spiral – galaxies: structure.

1 INTRODUCTION

The absence of a Keplerian decline in H I rotation curves that extend well beyond the stellar disc has provided compelling evidence that spiral galaxies are embedded within massive dark matter haloes (Bosma 1978; Begeman 1987). At the same time, it was noticed that the inner rotation curves can often be reproduced by the stellar disc alone, with a fairly similar disc mass-to-light ratio among spirals (Kalnajs 1983; Kent 1986; Freeman 1992; Palunas & Williams 2000). This coincidence has prompted the 'maximum-disc hypothesis', stating that the disc is as massive as allowed by the rotation curve (van Albada et al. 1985). However, the inner rotation curves are equally well reproduced with a submaximal disc and a more concentrated dark halo (van Albada et al. 1985; van der Kruit 1995; Broeils & Courteau 1997). An important development is that spirals of widely different disc central surface brightness follow the same Tully–Fisher relation (Zwaan et al. 1995; Verheijen 2001). This strongly implies that the disc contribution to the rotation curve decreases towards lower disc surface brightnesses (McGaugh &

⋆E-mail: vdkruit@astro.rug.nl

de Blok 1998). Of course, the behaviour with disc surface *density* remains unknown.

A promising tool suited for lifting this disc–halo degeneracy is the dynamical modelling of the stellar disc kinematics (van der Kruit & Freeman 1984, 1986; Bottema 1993; Pignatelli et al. 2001). This technique uses the principle of vertical dynamical equilibrium to constrain the actual disc surface density. Knowledge of the disc surface density will increase our understanding of the baryonic matter content of spiral galaxies and ultimately allow an investigation of the radial distribution of the dark matter. Important applications include the origin of the Tully–Fisher relation (McGaugh et al. 2000; Bell & de Jong 2001, hereafter BJ01; Freeman 2002) and the stability properties of discs, which are widely believed to regulate secular disc evolution (see Buta, Crocker & Elmegreen 1996, for reviews) and star formation (e.g. Wang & Silk 1994).

Bottema (1993, 1995, both hereafter B93) modelled the stellar kinematics of 11 normal (= unbarred) high surface brightness (HSB) spirals of predominantly late morphological type. Using the radial stellar velocity dispersion at one exponential disc scalelength as a reference, B93 found that spirals follow an approximately linear relation between stellar velocity dispersion and maximum rotational velocity. He then compared this σ versus $v_{\rm max}$ relation to that expected for an isolated exponential disc, assuming a disc flattening of 10 (the ratio of disc scalelength to scaleheight). Based on this comparison, he found that in normal HSB spirals the disc reaches 63 ± 10 per cent of the observed rotation at a radius of 2.2 disc scalelengths [the radius at which the rotation curve of an isolated exponential disc peaks (Freeman 1970)]. In other words, approximately 40 per cent of the mass enclosed within 2.2 disc scalelengths resides in the disc. In contrast, a working definition for the maximum contribution of the disc to the rotation is substantially higher at 85 ± 10 per cent (Sackett 1997). Note that the 63 per cent result is not based on either the disc colour or Freeman's law (Freeman 1970), as sometimes incorrectly stated (e.g. Bosma 1999).

In recent years, the question of the disc contribution to the rotation curve has also been addressed using several techniques other than using stellar kinematics. For two large independent samples, the Tully–Fisher residuals do not correlate with surface brightness (Courteau & Rix 1999). These authors argue that this observation requires a disc contribution of 60 ± 10 per cent in the majority of normal HSB spirals. In addition, the Tully–Fisher relation appears to be independent of barredness (Courteau et al. 2003), suggesting that barred and unbarred spirals have comparable fractions of luminous and dark matter. Maller et al. (2000) pointed out that constraints on the disc contribution are also provided by spirals that are strong gravitational lenses. By modelling both the lensing and the kinematics of the barred HSB spiral 2237+0305, Trott & Webster (2002) find a disc contribution of 57 ± 3 per cent. Fluid dynamical modelling of the gas structure and kinematics also constrains the disc contribution. These models seem to require a high disc mass-to-light ratio (M/L) and a rapidly rotating bar in both the Milky Way (Englmaier & Gerhard 1999) and NGC 4123 (Weiner, Sellwood & Williams 2001). Using this technique for normal spirals, Kranz, Slyz & Rix (2003) find that two massive HSB spirals, NGC 3893 and 5676, have maximum discs, whereas three less massive HSBs, NGC 3810, 4254 and 6643, are submaximal.

This is the final paper in a series[1] in which we address these issues and in general aim at providing new constraints on the dynamics of spiral galaxy discs through an observational synthesis of the global stellar disc structure and kinematics. The series is preceded by a reanalysis (Kregel, van der Kruit & de Grijs 2002, hereafter KKG) of the surface photometry in the I band of the sample of edge-on galaxies from de Grijs (1997, 1998). In Paper I in the series (Kregel, van der Kruit & Freeman 2004a), we presented optical spectroscopy to study the stellar kinematics in 17 edge-on galaxies mostly taken from the KKG sample. In Paper II (Kregel, van der Kruit & de Blok 2004b), we presented H I synthesis observations of 15 of these galaxies; and in Paper III (Kregel & van der Kruit 2004), we derived the circular velocity curves from the H I observations of Paper II and the optical emission-line (Hα) spectroscopy from Paper I. Comparison of the H I and Hα data shows that the effects of dust extinction on the derived stellar kinematics are small. In Paper IV (Kregel & van der Kruit 2005), we analysed the stellar disc kinematics of 15 edge-on spiral galaxies using a dynamical modelling technique in conjunction with the observed disc structure and rotation curves. For most of these, a transparent model provides a good match to the stellar disc kinematics. From this we determined the stellar velocity dispersion and the disc surface density at a fiducial radius of one I-band disc scalelength. In this final paper in the series, we first augment our discussion in KKG and study the correlations of the disc structural parameters with other global parameters, including the intrinsic disc flattening, for the full sample of 34 galaxies. We then study the stellar velocity dispersion and the stellar disc mass for the 15 spirals of Paper IV, and pay particular attention to their relation to the disc flattening and surface brightness.

This paper is organized as follows. First in Section 2 we discuss the correlation of the flattening of the stellar discs with other global properties in the KKG sample. The kinematic results, which were derived for a subsample of 15 galaxies, are analysed in Section 3. This includes a discussion on the velocity anisotropy (Section 3.1), the disc contribution to the rotation curve (Section 3.2), the σ versus $v_{\rm max}$ relation (Section 3.3), and the Tully–Fisher relation (Section 3.5). The most important results are summarized in Section 4.

2 THE DISC STRUCTURE

The spiral luminosity density of the discs is assumed to be axisymmetric and transparent and have the form

$$L_{\rm disc}(R, z) = L_0 \, {\rm e}^{-R/h_R} \, {\rm e}^{-z/h_z}, \tag{1}$$

where (R, z) are the cylindrical coordinates, L_0 is the central luminosity density, and h_R and h_z are the radial scalelength and the vertical scaleheight.

For a self-gravitating exponential disc, there is a simple relation between its peak rotational velocity ($v_{\rm disc}$, at $2.2\,h_R$), central surface density (Σ_0) and scalelength (Freeman 1970):

$$v_{\rm disc} = 0.88\sqrt{\pi G \Sigma_0 h_R}, \tag{2}$$

where G is the gravitational constant. For a self-gravitating disc in vertical dynamical equilibrium, the surface density $\Sigma\,(R) = \Sigma_0 \exp(-R/h_R)$ is related to the scaleheight of the disc mass distribution and the vertical stellar velocity dispersion (σ_z) through the Jeans equation for vertical hydrostatic equilibrium:

$$\sigma_z(R) = \sqrt{C G \Sigma(R) h_z}. \tag{3}$$

Here C is a constant depending on the detailed form of the vertical density distribution: for an exponential distribution, $C = 3\pi/2$; for a sech dependence, $C = 1.71\pi$; and for an isothermal distribution, $C = 2\pi$ (van der Kruit 1988). When the surface density from equation (3), evaluated at the centre, is substituted into equation (2), a simple

[1] The series contains adapted versions of most chapters in the PhD thesis of MK (Kregel 2003).

Table 1. Photometric parameters.

Galaxy	$\mu_{0,I}^{\text{edge-on}}$ (mag arcsec^{-2})	$h_{R,I}$ (arcsec)	$h_{z,I}$ (arcsec)	h_R/h_z	$\mu_{0,I}^{\text{face-on}}$ (mag arcsec^{-2})
(1)	(2)	(3)	(4)	(5)	(6)
ESO 026-G06	20.4 ± 0.1	26.0 ± 1.5	3.7 ± 0.3	7.0 ± 0.7	22.3 ± 0.2
ESO 033-G22	19.8 ± 0.3	18.3 ± 5.0	2.0 ± 0.2	9.2 ± 2.7	22.0 ± 0.3
ESO 041-G09	19.8 ± 0.2	34.6 ± 3.0	3.9 ± 0.3	8.9 ± 1.0	21.9 ± 0.2
ESO 138-G14	21.6 ± 0.2	41.7 ± 3.5	6.0 ± 0.6	7.0 ± 0.9	23.5 ± 0.3
ESO 141-G27	20.3 ± 0.2	40.4 ± 4.0	4.1 ± 0.4	9.9 ± 1.4	22.7 ± 0.2
ESO 142-G24	19.7 ± 0.2	36.8 ± 2.7	3.8 ± 0.2	9.7 ± 0.9	22.1 ± 0.2
ESO 157-G18	19.8 ± 0.2	36.5 ± 2.2	4.8 ± 0.3	7.6 ± 0.7	22.0 ± 0.2
ESO 201-G22	19.3 ± 0.2	24.3 ± 2.5	2.9 ± 0.4	8.4 ± 1.4	21.6 ± 0.2
ESO 202-G35	18.3 ± 0.2	22.8 ± 2.3	3.6 ± 0.4	6.3 ± 1.0	20.3 ± 0.3
ESO 240-G11	18.4 ± 0.4	49.0 ± 9.0	3.5 ± 0.8	14.0 ± 4.1	21.3 ± 0.4
ESO 263-G15	17.6 ± 0.2	31.2 ± 1.6	2.9 ± 0.2	10.8 ± 0.9	19.7 ± 0.2
ESO 263-G18	18.4 ± 0.2	27.7 ± 2.6	3.2 ± 0.5	8.7 ± 1.6	20.5 ± 0.2
ESO 269-G15	19.1 ± 0.3	29.0 ± 5.2	4.2 ± 0.6	6.9 ± 1.6	21.0 ± 0.3
ESO 288-G25	17.6 ± 0.4	18.4 ± 4.0	2.5 ± 0.4	7.4 ± 2.0	19.8 ± 0.4
ESO 315-G20	19.9 ± 0.3	22.9 ± 5.0	2.7 ± 0.6	8.5 ± 2.6	22.2 ± 0.3
ESO 321-G10	19.1 ± 0.2	20.5 ± 4.1	2.9 ± 0.3	7.1 ± 1.6	21.1 ± 0.3
ESO 322-G87	18.1 ± 0.4	16.8 ± 3.5	2.6 ± 0.4	6.5 ± 1.7	19.9 ± 0.4
ESO 340-G08	19.1 ± 0.1	11.5 ± 2.8	1.4 ± 0.2	8.2 ± 2.3	21.3 ± 0.2
ESO 340-G09	20.3 ± 0.3	22.5 ± 3.5	3.5 ± 0.5	6.4 ± 1.4	22.3 ± 0.3
ESO 416-G25	20.0 ± 0.1	22.7 ± 2.0	3.8 ± 0.4	6.0 ± 0.8	21.9 ± 0.2
ESO 435-G14	18.3 ± 0.4	17.6 ± 3.4	3.3 ± 0.3	5.3 ± 1.1	20.0 ± 0.5
ESO 435-G25	19.1 ± 0.4	97.0 ± 19.0	5.0 ± 0.3	19.4 ± 4.0	22.2 ± 0.4
ESO 435-G50	20.1 ± 0.1	13.2 ± 1.5	1.7 ± 0.3	7.8 ± 1.6	22.2 ± 0.2
ESO 437-G62	18.9 ± 0.5	35.8 ± 3.7	6.6 ± 0.5	5.4 ± 0.7	20.6 ± 0.5
ESO 446-G18	19.1 ± 0.1	25.8 ± 3.0	2.0 ± 0.1	12.9 ± 1.6	21.8 ± 0.1
ESO 446-G44	19.0 ± 0.2	31.1 ± 2.1	2.8 ± 0.2	11.1 ± 1.1	21.5 ± 0.2
ESO 460-G31	19.2 ± 0.3	28.1 ± 4.6	2.4 ± 0.4	11.7 ± 2.7	21.6 ± 0.3
ESO 487-G02	18.4 ± 0.3	24.3 ± 1.9	3.8 ± 0.4	6.4 ± 0.8	20.4 ± 0.3
ESO 506-G02	19.2 ± 0.1	19.4 ± 4.0	2.8 ± 0.4	6.9 ± 1.7	21.1 ± 0.2
ESO 509-G19	19.1 ± 0.5	24.8 ± 4.0	2.5 ± 0.5	9.9 ± 2.5	21.5 ± 0.5
ESO 531-G22	18.4 ± 0.4	19.8 ± 4.0	3.1 ± 0.5	6.4 ± 1.7	20.4 ± 0.4
ESO 555-G36	20.2 ± 0.2	10.9 ± 1.4	2.8 ± 0.3	3.9 ± 0.7	21.5 ± 0.3
ESO 564-G27	19.6 ± 0.2	38.0 ± 5.1	3.5 ± 0.4	10.9 ± 1.9	22.0 ± 0.2
ESO 575-G61	20.2 ± 0.2	16.2 ± 1.3	2.7 ± 0.4	6.0 ± 1.0	22.1 ± 0.3

(1) Galaxy. (2) Edge-on central surface brightness $\mu_{0,I}^{\text{edge-on}}$. (3) Scalelength $h_{R,I}$. (4) Scaleheight $h_{z,I}$. (5) Flattening h_R/h_z. (6) Face-on central surface brightness $\mu_{0,I}^{\text{face-on}}$.

relation between the maximum rotation, central velocity dispersion and flattening of the disc is obtained:

$$v_{\text{disc}} = (0.69 \pm 0.03)\sigma_z|_{R=0} \sqrt{h_R/h_z}. \quad (4)$$

Here the constant accounts for density laws ranging from an exponential to a sech dependence.

2.1 Disc structure and global parameters

In KKG we analysed *I*-band photometry of 34 edge-on spiral galaxies taken from the sample of de Grijs (1998) to study the global structure of the old stellar discs. The exponential scale parameters and the central surface brightness of the disc light were derived using a 2D least-squares fitting method. This procedure includes a bulge–disc decomposition and adopts a mask to exclude systematically the region affected by dust and young populations. We derived for the stellar discs the photometric *I*-band parameters: edge-on central surface brightness $\mu_I^{\text{edge-on}}$, radial scalelength h_R and vertical scaleheight h_z. These and the derived flattening h_R/h_z and face-on central surface brightness $\mu_I^{\text{face-on}}$ are listed in Table 1. The face-on surface brightnesses were obtained using

$$\mu^{\text{face-on}} = \mu^{\text{edge-on}} + 2.5 \log_{10}(h_R/h_z)$$

and correcting for Galactic extinction as in de Grijs (1998). Note that in the original paper of KKG the edge-on surface brightnesses for 10 galaxies are in error due to incorrect zero-points. Table 1 lists the correct values for the edge-on central surface brightness.

Both scale parameters and their ratio are plotted as a function of the galaxy maximum rotational velocity according to LEDA in Figs 1(a)–(c) (see also KKG), and against the face-on central surface brightness of the disc in Figs 1(d)–(f). The range in face-on central surface brightness is about four magnitudes (e.g. Fig. 1d), reaching well into the low surface brightness (LSB) regime. The brightest discs appear to have $\mu_{0,I} \simeq 20$ mag arcsec^{-2}. This is roughly a magnitude fainter than observed in less-inclined spirals (Verheijen 1997; de Jong & Lacey 2000), probably signalling an underestimation of the face-on surface brightness for at least the HSB discs. This may be related to the uncertainty in the shape of the vertical

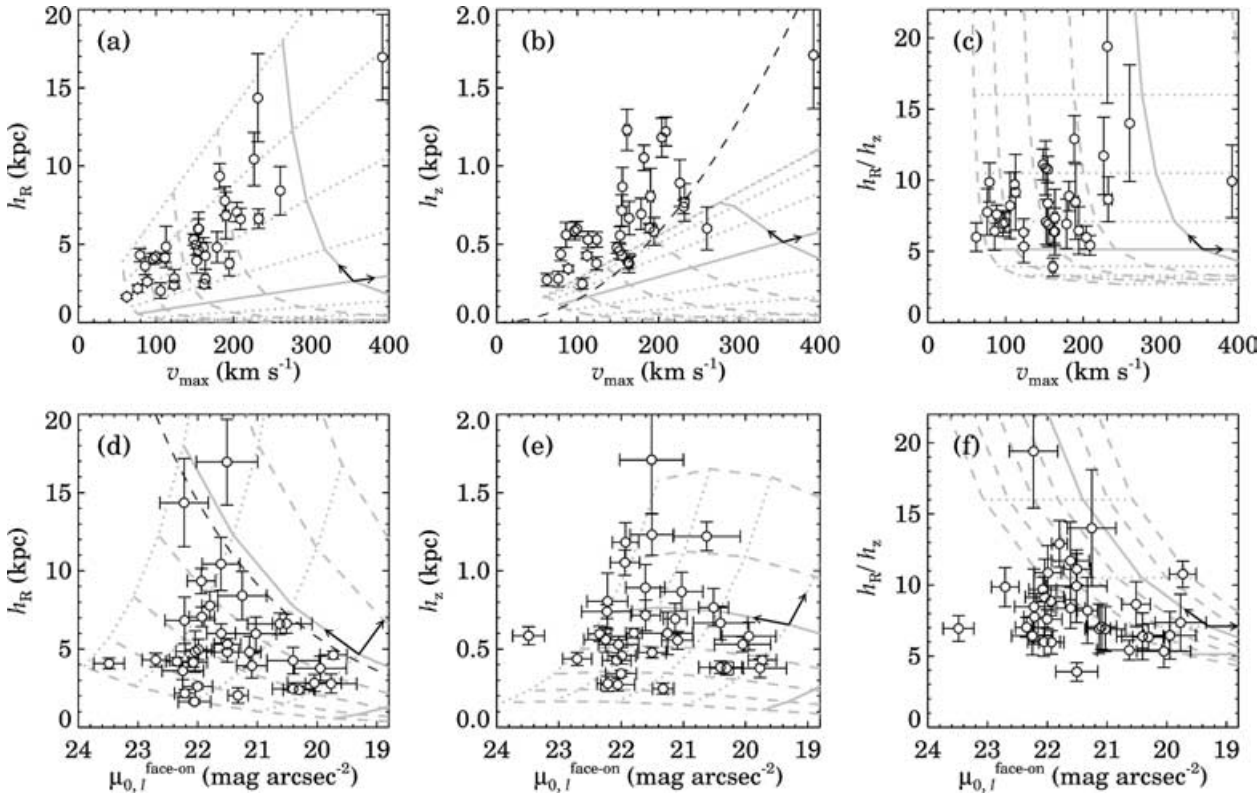

Figure 1. The disc scalelength, scaleheight and flattening as functions of maximum rotational velocity (a)–(c) and face-on central surface brightness (d)–(f). The black dashed line in (d) is the relation for exponential discs with luminosity $L_\star = 4 \times 10^{10}\,\mathrm{L}_{\odot,I}$. In each panel, the grey lines show the collapse model for disc galaxy formation, the dashed lines connect models of the same total mass [$\log_{10}(M_{\rm tot}) = 10$–$13$ in steps of 0.5, and the solid line at $\log_{10}(M_{\rm tot}) = 12$] and dotted lines connect models with the same spin parameter (logarithmically spaced, separated by factors of 0.2 dex, solid line at $\lambda = 0.06$). Arrows indicate the direction of increasing $M_{\rm tot}$ and λ.

light distribution close to the plane and/or residual dust extinction (KKG).

As seen in studies of face-on spirals, the disc scalelength increases with maximum rotational velocity (Fig. 1a, originally found by van der Kruit & de Grijs 1999) and tends to be smaller for a higher face-on central surface brightness (Fig. 1d). In essence, these correlations are a reflection of the fact that spirals follow a single Tully–Fisher relation, irrespective of their central surface brightness (Zwaan et al. 1995; Verheijen 2001). The tendency of HSB discs to have smaller scalelengths is a manifestation of the exponential cut-off of the luminosity function of spirals; the black dashed line in Fig. 1(d) indicates the relation expected for $L_\star = 4 \times 10^{10}\,\mathrm{L}_{\odot,I}$ (de Jong & Lacey 2000). HSB discs with large scalelengths do not appear to exist. Of equal interest is the tight correlation found between the scaleheight and $v_{\rm max}$ (Fig. 1b, originally found by van der Kruit & de Grijs 1999). A Spearman rank correlation test yields a correlation coefficient $R_{\rm S} = 0.74$ (greater than 99 per cent confidence). Apparently, spiral galaxies with a higher maximum rotation have both larger *and* thicker discs. The most extreme example of this is ESO 509-G19. This huge spiral has an extremely large maximum rotational velocity of 392 km s^{-1} and a disc scalelength and scaleheight of 17 kpc and 1.7 kpc, respectively. A least-squares bisector fit (Isobe et al. 1990) to the relation gives

$$h_z = (0.45 \pm 0.05)(v_{\rm max}/100\,\mathrm{km\,s^{-1}}) + (-0.14 \pm 0.07)\ \mathrm{kpc}$$

and an observed scatter of 0.21 kpc. This may be used to estimate the scaleheight of spirals that are less inclined.

In Fig. 2 we show the disc structural parameters versus the total H I mass and the H I richness (the ratio of the H I mass to the total disc luminosity). The trends are similar to those in Fig. 1, showing a definite increase of the scalelength and scaleheight with H I content and a (tentative) decrease with H I richness. Figs 1(c) and 2(c) appear to show that there are no slowly rotating, highly flattened spirals. The observed lack of these spirals may be due to the selection against small and LSB spirals imposed by the diameter limit. Indeed, the *B*-band isophotal axial ratios of the galaxies in the Revised Flat Galaxy Catalog (RFGC; Karachentsev et al. 1999), selected using a substantially smaller diameter limit, show no evidence for a correlation with maximum rotational velocity (Zasov et al. 2002). The current data do show a weak correlation between disc flattening and face-on central surface brightness (Fig. 1f, $R_{\rm S} = -0.27$ or 90 per cent confidence); on average LSB discs tend to be more flattened. It should be stressed here that the diameter limit causes a selection against LSB discs, especially those which are less flattened: since

$$\mu^{\rm edge\text{-}on} = \mu^{\rm face\text{-}on} - 2.5\log_{10}(h_R/h_z)$$

the selection is strongest against low face-on surface brightness (LSB) discs that are fat. We do, however, observe a significant number of fat LSB discs. This suggests that fat LSB discs are more common than flat LSB discs. In any event, highly flattened discs of high face-on surface brightness should clearly stand out in a diameter-limited sample. The fact that these are not observed (Fig. 1f) indicates that the trend between disc flattening and face-on surface

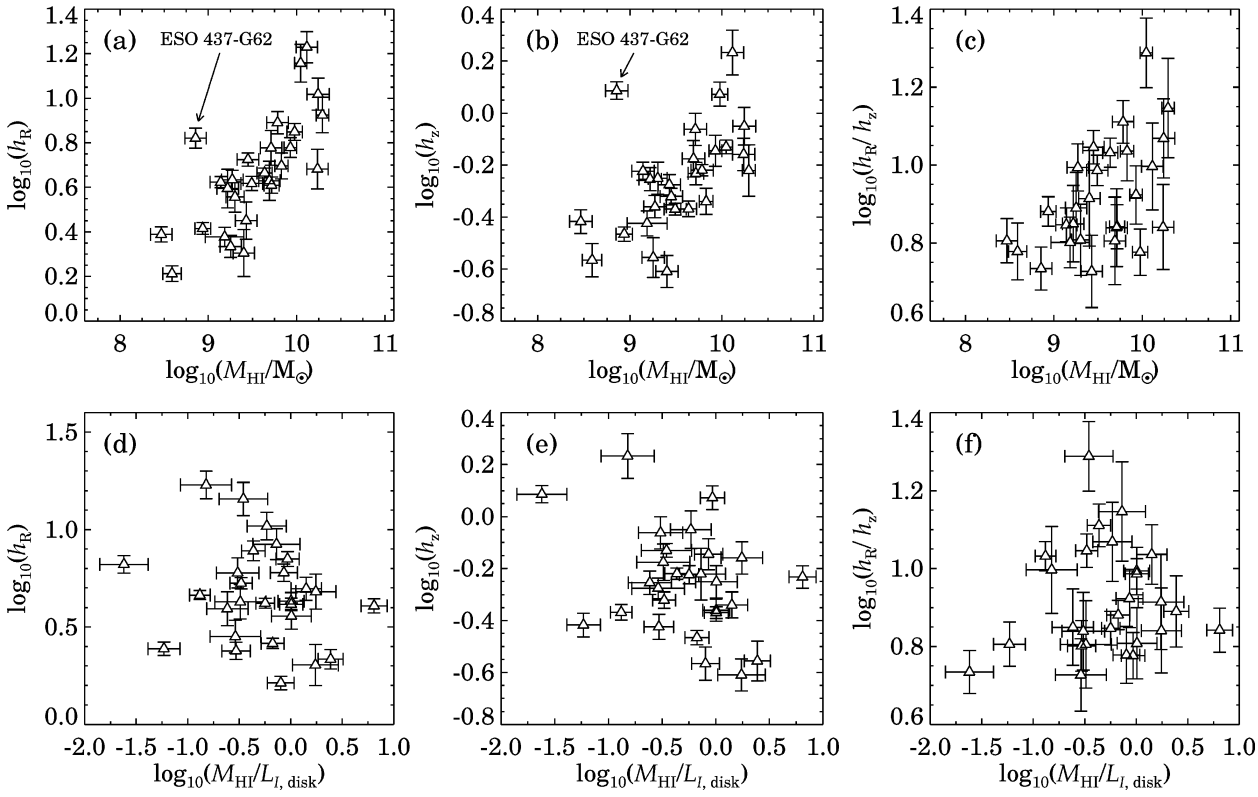

Figure 2. The disc scale parameters versus total H I mass (a)–(c) and H I richness (d)–(f). The H I masses were calculated using the integrated H I fluxes from LEDA and assuming that H I is optically thin. Note that ESO 437-G62 is classified Sb in LEDA, but given its very low H I mass is probably a lenticular.

brightness is probably real. We note that similar but tighter relations have been reported for two samples drawn from the RFGC (Bizyaev & Mitronova 2002; Zasov et al. 2002), based on *R*-band photometry and 2MASS K_s-band images. Perhaps these tighter relations are the result of different selection criteria; the galaxies in the RFGC were selected to have *B*-band optical diameters larger than 40 arcsec and isophotal axial ratios $a/b \geqslant 7$ (Karachentsev et al. 1999), favouring intrinsically small galaxies of late morphological type.

The analytical collapse model of disc galaxy formation incorporates a range of central surface brightnesses, providing a simple framework for trying to understand the observed trends (Fall & Efstathiou 1980; Gunn 1982; Dalcanton, Spergel & Summers 1997, hereafter DSS97; Mo, Mao & White 1998). In this picture, discs form through dissipational collapse of the baryonic matter within virialized dark matter haloes. The collapse of the baryons is halted depending on the amount of angular momentum imprinted on the haloes in the early Universe, and the baryons settle in a rapidly rotating disc. Under the basic assumption of detailed angular momentum conservation throughout the collapse, the model predicts the final disc radial surface density profile and the galaxy rotation curve as a function of the total mass $M_{\rm tot}$ and the spin parameter λ (Peebles 1969) of the protogalaxy,

$$\lambda = J|E|^{1/2}G^{-1}M^{-5/2}, \tag{5}$$

where J is the total angular momentum, E the total energy and M the total mass. We used the prescription of DSS97 to calculate these over a range in total mass, $M_{\rm tot} = 10^{10}$–$10^{13}\,{\rm M}_\odot$, and spin parameter, $\lambda = 0.01$–0.28. The latter range was adopted based on the spin parameters of the collapsed dark matter haloes in cold dark matter simulations. These simulations consistently reveal an approximately log-normal distribution of spin parameters with a mean $\langle\lambda\rangle \simeq 0.04$ and a width $\log\sigma_\lambda \simeq 0.5$ (Warren et al. 1992; Bullock et al. 2001a). We used a fixed baryonic mass fraction $F = 0.10$, a Hernquist halo at the onset of baryon decoupling (as in DSS97) and $H_0 = 75\,{\rm km\,s^{-1}\,Mpc^{-1}}$. Surface brightness and luminosity are calculated assuming that the efficiency for turning the baryons into stars over the age of the disc is constant among galaxies at $(M/L)_{\rm disc} = 2$.

In the collapse model, both h_R and $v_{\rm max}$ increase as $M_{\rm tot}^{1/3}$, yielding a linear relation for a constant spin parameter (Fig. 1a). The region in the h_R versus $v_{\rm max}$ plane occupied by the models is in general agreement with the data, and suggests that the observed discs arise from haloes with higher-than-average λ. This is irrespective of the adopted baryonic fraction, but may be a manifestation of the selection against small galaxies. The model is also able roughly to match the observed scalelength–central surface brightness distribution (Fig. 1d); at constant $M_{\rm tot}$ the baryons within less rapidly spinning haloes collapse further inwards, yielding higher surface brightness discs with smaller scalelengths (DSS97).

The scaleheights of the model discs were estimated as follows. Numerical simulations suggest that galaxy discs are on the verge of instability (Hohl 1971; Sellwood & Carlberg 1984; Athanassoula & Sellwood 1986; Mihos, McGaugh & de Blok 1997; Bottema 2003), having stellar velocity dispersions that are a constant multiple of the critical velocity dispersion for local stability. In terms of Toomre's stability criterion Q (Toomre 1964, see equation 11 below), the radial velocity dispersion is

$$\sigma_R = Q\frac{3.36\Sigma}{\kappa}, \tag{6}$$

where κ is the epicyclic frequency (from the rotation curve), and the simulations suggest $Q = 1.5$–2.5. Hence, for an assumed Q, the collapse model predicts the radial stellar velocity dispersion. Hence,

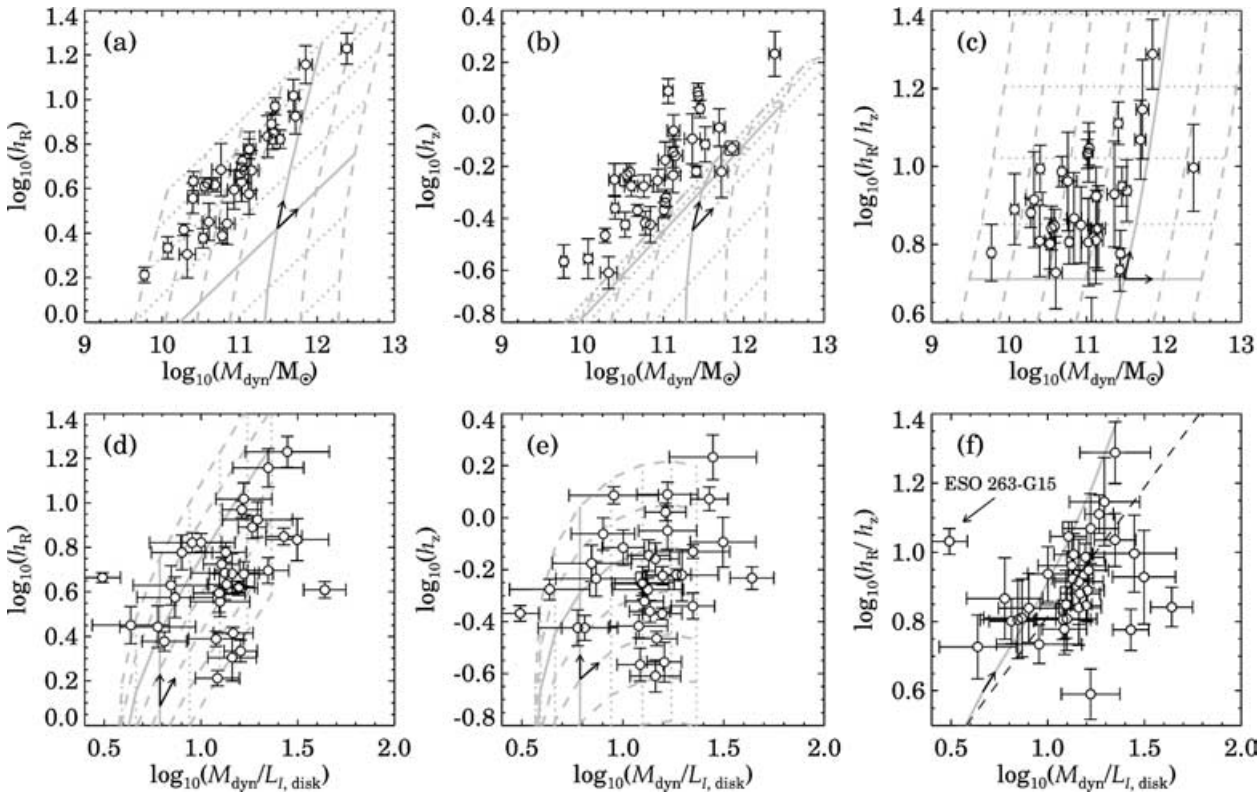

Figure 3. The disc scalelength, scaleheight and flattening as functions of dynamical mass (a)–(c) and the ratio of dynamical mass to disc luminosity (d)–(f). The grey lines are as in Fig. 1. The dashed line in (f) indicates the least-squares bisector fit.

for discs in vertical dynamical equilibrium (equation 3), an estimate of the ratio of the vertical to the radial velocity dispersion (σ_z/σ_R) gives a prediction for the scaleheight. Combining equations (3) and (6) for a vertically exponential disc:

$$h_z = \left(\frac{3.36 Q \sigma_z}{\sigma_R}\right)^2 \frac{\Sigma}{\frac{3}{2}\pi G \kappa^2}. \quad (7)$$

With this semi-empirical approach, scaleheights were calculated at a radial distance of one scalelength, adopting $Q = 2.5$ and the solar neighbourhood value $\sigma_z/\sigma_R = 0.6$ (Dehnen & Binney 1998; Mignard 2000). Note that the validity of such a constant product ($Q\sigma_z/\sigma_R$) is certainly questionable. Disc heating theory suggests that the range in σ_z/σ_R is small among spirals, about 0.4–0.8 (Jenkins & Binney 1990), consistent with the (scarce) observational evidence (Gerssen, Kuijken & Merrifield 2000; Shapiro, Gerssen & van der Marel 2003). However, taking an uncertainty of a factor of 2 for Q already gives a huge range in possible model scaleheights. Considering that the assumption of disc self-gravity underlies equation (3), this further underlines that the model cannot be expected to match the observations exactly at low surface brightness. Nevertheless, this simple model provides a useful starting point to investigate possible trends with scaleheight and flattening.

Like the scalelengths, the scaleheights increase as $M_{\rm tot}^{1/3}$, such that in Fig. 1b the model shows a behaviour similar to that in the h_R versus $v_{\rm max}$ plane. However, for the adopted ($Q\sigma_z/\sigma_R$), the sizes of the observed scaleheights are underpredicted by a factor of 2. A σ_z/σ_R around 0.8 could explain this discrepancy, but is unexpected for late-type spirals (Gerssen et al. 2000; Shapiro et al. 2003). Taking a Q value higher than that reached in the simulations would also work. Alternatively, a higher baryonic mass fraction could raise the disc surface density and hence the scaleheight. However, the adopted $F = 0.10$ is also already on the high side considering that conservative upper limits based on extended H I rotation curves require $F \lesssim 0.05$ (McGaugh & de Blok 1998).

An interesting feature of the collapse model is that the disc flattening is solely driven by the spin parameter. Haloes with higher spin produce discs that have not only a lower surface brightness but also a higher flattening, independent of $M_{\rm tot}$. This is in qualitative agreement with the data (Fig. 1f). This is remarkable because any systematic change in ($Q\sigma_z/\sigma_R$) with surface brightness could easily alter the trend [the flattening goes as $(Q\sigma_z/\sigma_R)^{-2}$]. Therefore, at least the range in ($Q\sigma_z/\sigma_R$) is approximately constant among discs with different surface brightness. Note that the model predicts the existence of small, highly flattened spirals (Fig. 1c). This is the case for a large range in ($Q\sigma_z/\sigma_R$) and F, suggesting that the lack of these systems in our sample is indeed a selection effect.

To investigate the trends with the global dynamics, Fig. 3 displays in logarithmic units the structural parameters versus the dynamical mass and the ratio of dynamical mass to disc luminosity. The dynamical mass is defined as the total mass enclosed within four scalelengths (assuming sphericity),

$$M_{\rm dyn} = 4 h_R v_{\rm max}^2 / G. \quad (8)$$

The disc luminosity is $L_{\rm disc} = 2\pi h_R^2 \mu_0^{\rm face\text{-}on}$. Both the scalelength and scaleheight show a tight correlation with dynamical mass, as expected from Figs 1(a) and (b). The disc scalelength also tends to be larger for spirals with a higher dynamical mass-to-light ratio (Fig. 3d, $R_{\rm S} = 0.49$ or a confidence level greater than 99 per cent). A less clear trend is observed between scaleheight

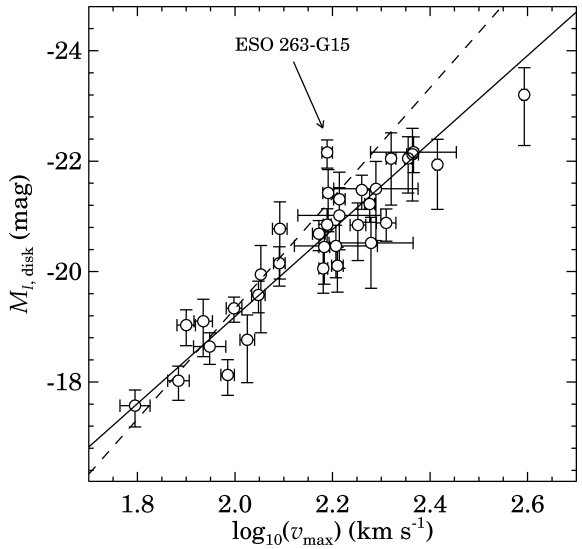

Figure 4. The disc luminosity Tully–Fisher relation. The solid line indicates the least-squares bisector fit. The dashed line indicates the *I*-band TF according to the *HST* Key Project (Sakai et al. 2000).

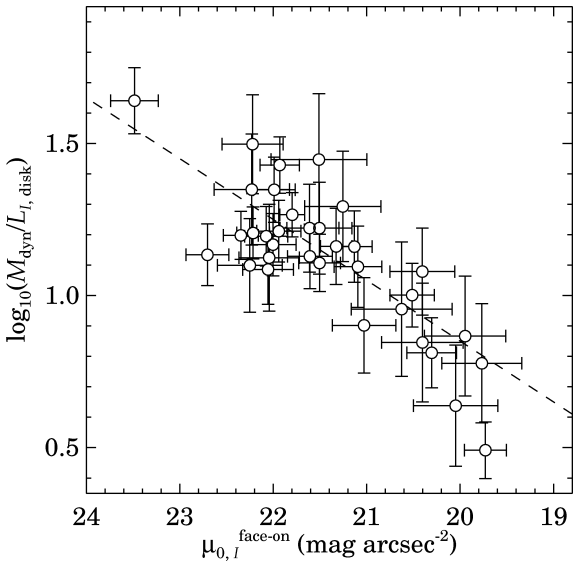

Figure 5. The dynamical mass to disc luminosity ratio versus the face-on central surface brightness of the disc. The dashed line indicates an $M_{\mathrm{dyn}}/L \propto \mu_0^{-1/2}$ relation, arbitrarily shifted in zero-point to match the observed relation.

and dynamical mass-to-light ratio (Fig. 3e, $R_{\mathrm{S}} = 0.33$ or 94 per cent confidence). The disc flattening appears to show an increase towards higher masses. As for v_{max} (Fig. 1c), this trend is probably artificial.

The disc flattening shows a genuine trend with dynamical mass-to-light ratio (Fig. 3f, $R_{\mathrm{S}} = 0.48$ at greater than 99 per cent confidence). More flattened discs tend to reside in spiral galaxies with larger dynamical mass-to-light ratio, i.e. in which the luminous disc is less important dynamically [provided that $(M/L)_{\mathrm{disc}}$ does not strongly increase with dynamical mass-to-light ratio]. The trend is similar to those found in the *R* and K_{s} bands by Zasov et al. (2002) and to that of the simple collapse model. Interestingly, the collapse model reduces to a single line with a logarithmic slope of unity; both the inferred disc flattening and dynamical mass-to-light ratio are independent of M_{tot} but increase with increasing spin parameter. A simple linear least-squares bisector fit to the entire sample gives a logarithmic slope 0.75 ± 0.11 and a 1σ scatter of 0.2 dex (as a result of the uncertainties in the disc luminosities of edge-on spirals, the zero-point cannot be reliably determined). Note that the outliers also deviate strongly from the disc Tully–Fisher relation (Fig. 4, e.g. ESO 263-G15). Perhaps the distances to these spirals are seriously in error.

2.2 Disc structure and the Tully–Fisher relation

The observation that disc flattening correlates with both dynamical mass-to-light ratio and surface brightness is probably rooted in the Tully–Fisher (TF) relation. Fig. 4 shows the TF relation, using the disc luminosity derived here and the maximum rotation according to LEDA. A least-squares bisector fit (solid line) gives a slope[2] $\alpha = 3.2 \pm 0.2$ and an intercept $\log_{10}(L_{100}/\mathrm{L}_{\odot}) = 9.33 \pm 0.03$. This relation lies systematically below the *HST* Key Project *I*-band TF relation (dashed line), which refers to the total luminosities and has a slope $\alpha = 4.0$ and an intercept $\log_{10}(L_{100}/L_{\odot}) = 9.39$ (Sakai et al. 2000). The offset is a complicated issue and will be further pursued in Section 3 using v_{max} derived from full H I synthesis rotation curves. An important ingredient for the present discussion is that spirals lie on the same TF relation irrespective of their disc surface brightness (Zwaan et al. 1995; Verheijen 2001). This implies that the product $(M_{\mathrm{dyn}}/L_{\mathrm{disc}})^2 \mu_0^{\mathrm{face\text{-}on}}$ (with μ in linear units) is a constant among spirals, provided that the disc TF relation has a slope close to 4 (Zwaan et al. 1995; McGaugh & de Blok 1998; Graham 2002). The relation between $M_{\mathrm{dyn}}/L_{\mathrm{disc}}$ and $\mu_0^{\mathrm{face\text{-}on}}$ for the present sample is shown in Fig. 5. The data are indeed consistent with a tight relation $M_{\mathrm{dyn}}/L_{\mathrm{disc}} \propto \mu_0^{-1/2}$, as in face-on systems (de Blok, McGaugh & van der Hulst 1996).

For an exponential disc, the ratio of the peak rotation velocity of the disc (equation 2) to the maximum rotation velocity ($v_{\mathrm{disc}}/v_{\mathrm{max}}$) is

$$\frac{v_{\mathrm{disc}}}{v_{\mathrm{max}}} = \frac{0.880(\pi G \Sigma_0 h_R)^{1/2}}{v_{\mathrm{max}}}. \quad (9)$$

This is related to the ratio of the disc mass M_{disc} to the total mass M_{dyn}, which according to equation (8) is $M_{\mathrm{disc}}/M_{\mathrm{dyn}} \propto (v_{\mathrm{disc}}/v_{\mathrm{max}})^2|_{2.2\,h_R}$. Together with the increase of $M_{\mathrm{dyn}}/L_{\mathrm{disc}}$ with decreasing surface brightness, this suggests that the disc contribution to the rotation curve (equation 9) declines continuously with decreasing surface brightness. The requirement is that the disc mass-to-light ratio $(M/L)_{\mathrm{disc}}$ is not strongly increasing with decreasing surface brightness. Stellar population synthesis models do indicate a relation between the stellar $(M/L)_{\mathrm{disc}}$ ratio and surface brightness (BJ01), but this relation is relatively weak and has the opposite sign (see McGaugh & de Blok 1998, for a discussion). In a similar fashion, Fig. 3(f) indicates that the disc contribution to the rotation curve decreases with increasing flattening. The observed relation between disc flattening and dynamical mass-to-light ratio may be used with the general equation (4) to estimate the stellar velocity dispersion as a function of disc flattening. Unfortunately, also here the zero-point is difficult to determine given the uncertainties in the disc luminosities. Still, taking the bisector fit for the disc flattening

[2] $L/\mathrm{L}_{\odot} = (L_{100}/\mathrm{L}_{\odot})\,[v_{\mathrm{max}}/(100\,\mathrm{km\,s^{-1}})]^{\alpha}$, $\mathrm{M}_{\odot,I} = 4.14$.

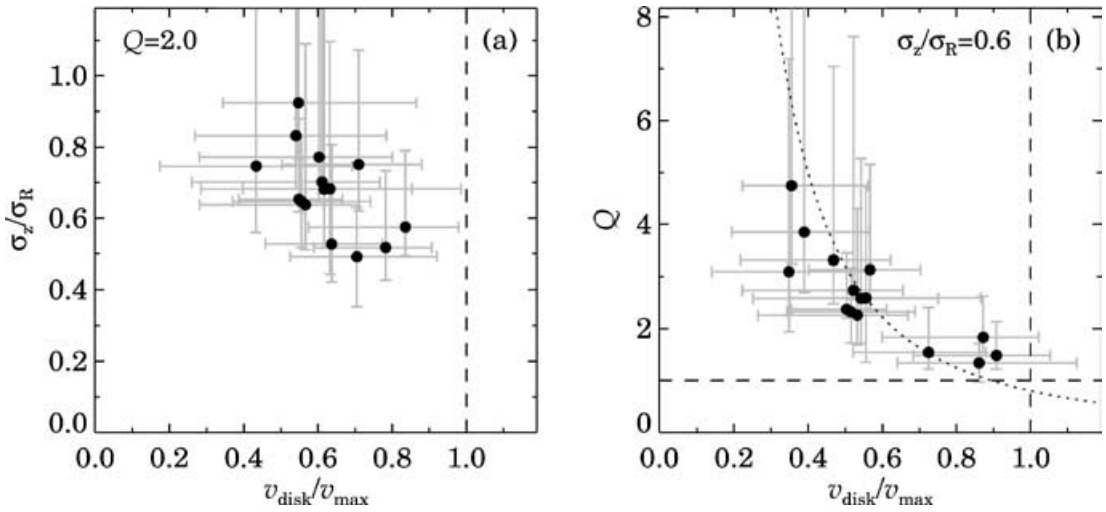

Figure 6. (a) The velocity anisotropy at one disc scalelength versus the disc contribution to the rotation curve for constant $Q = 2.0$. (b) Plot of Q at one scalelength versus the disc contribution to the rotation curve for constant $\sigma_z/\sigma_R = 0.6$. The dotted line shows $Q \propto (v_{\rm disc}/v_{\rm max})^{-2}$ (not a fit).

versus $M_{\rm dyn}/L_{\rm disc}$ (Fig. 3f) and using $M_{\rm dyn}/L_{\rm disc} \propto \mu_0^{-1/2}$, we get

$$\sigma_z(0) \propto \left(\frac{h_R}{h_z}\right)^{-1.17} \left(\frac{M}{L}\right)^{1/2}_{\rm disc} v_{\rm max} \propto \mu_0^{0.44} \left(\frac{M}{L}\right)^{1/2}_{\rm disc} v_{\rm max}, \quad (10)$$

with μ_0 in linear units. The important implication is that at a constant $v_{\rm max}$ (or luminosity) the vertical stellar disc velocity dispersion decreases with increasing flattening or, equivalently, with decreasing central surface brightness. This prediction holds for self-gravitating discs as long as the disc M/L does not strongly increase with decreasing surface brightness. The behaviour of equation (10) is very similar to that predicted by Bottema (1997) on the basis of a relation between disc mass-to-light ratio and broadband colour.

3 DISC DYNAMICS

In Paper IV we fitted the observations of the stellar kinematics to a model of the disc dynamics. These fits resulted essentially in a property $\sqrt{M/L}\,(\sigma_z/\sigma_R)^{-1}$, a combination of the (square root of the) disc mass-to-light ratio and the velocity anisotropy. Through an assumed σ_z/σ_R, this property can be used to study the disc surface density. It is important to note that for edge-on systems the dynamical model is unable to provide tight constraints on the disc M/L because of the uncertainty in the disc central surface brightness (see section 3.2 of Paper IV for details).

3.1 The velocity anisotropy

In the solar neighbourhood the velocity anisotropy is $\sigma_z/\sigma_R = 0.53 \pm 0.07$ (Dehnen & Binney 1998; Mignard 2000). Recently, it has also been measured in five spirals of type Sa to Sbc (Gerssen, Kuijken & Merrifield 1997; Gerssen et al. 2000; Shapiro et al. 2003), giving σ_z/σ_R in the range 0.6–0.8. These values are broadly consistent with the theory of dynamical heating in isolated discs (Gerssen et al. 2000; Shapiro et al. 2003), which predicts that σ_z/σ_R is larger in discs with less pronounced spiral structure (Jenkins & Binney 1990). The anisotropy is related to the flattening of the disc (van der Kruit & de Grijs 1999).

3.1.1 Disc stability

Toomre's criterion (Toomre 1964) states that local axisymmetric perturbations in an infinitely thin stellar disc are suppressed at all length-scales by either differential rotation or random motion when

$$Q \equiv \frac{\sigma_R \kappa}{3.36 G \Sigma} \quad (11)$$

exceeds unity. Here κ is the epicyclic frequency ($\sqrt{2}\,v_c/R$ for a flat rotation curve) and Σ the disc surface density. From modelling the observed stellar kinematics, the surface density ($=\mu_0 M/L$) is known up to a factor $(\sigma_z/\sigma_R)^2$. Hence, independent knowledge of Q can be used with the stellar dispersions and the rotation curves to estimate σ_z/σ_R. Simulated discs that prove stable evolve to Q values in the range 1.5–2.5 (Hohl 1971; Sellwood & Carlberg 1984; Athanassoula & Sellwood 1986; Mihos et al. 1997; Bottema 2003), with the lower bound corresponding to more massive discs (relative to the halo). These values agree with stability criteria that take into account that a disc is more unstable to non-axisymmetric perturbations (Griv et al. 1999).

Fig. 6(a) shows for each galaxy at one disc scalelength the velocity anisotropy modelled in Paper IV, assuming that $Q = 2.0$ for all discs, as a function of $v_{\rm disc}/v_{\rm max}$ (equation 9). The anisotropies in Fig. 6(a) have an average value of 0.67 and a 1σ scatter of 0.12. Obviously, for different Q the inferred average changes: for Q in the range 1.5–2.5, the average σ_z/σ_R is in the range 0.77–0.60. Fig. 6(a) further hints that the anisotropy decreases with increasing disc contribution. For discs that appear close to maximal ($v_{\rm disc}/v_{\rm max} > 0.75$), the anisotropy appears to be $\sigma_z/\sigma_R \sim 0.5$, while for strongly submaximal discs $\sigma_z/\sigma_R \sim 0.8$. Such a trend is present independent of the Q value, as long as Q is constant.

If spiral structure and molecular clouds are the prime agents for disc heating, σ_z/σ_R will decrease from $\simeq$0.75 for heating by clouds alone to $\simeq$0.45 as spiral structure becomes more and more important (Jenkins & Binney 1990). This range is in agreement with Fig. 6(a). Unfortunately, in edge-on systems it is difficult to verify whether a decrease in σ_z/σ_R is associated with an increasing importance of spiral structure. The observed trend does appear to fit in with swing-amplification theory, which predicts that spiral structure is stronger in discs with a larger contribution to the rotation (Toomre 1981; Athanassoula, Bosma & Papaioannou 1987). Qualitatively, more

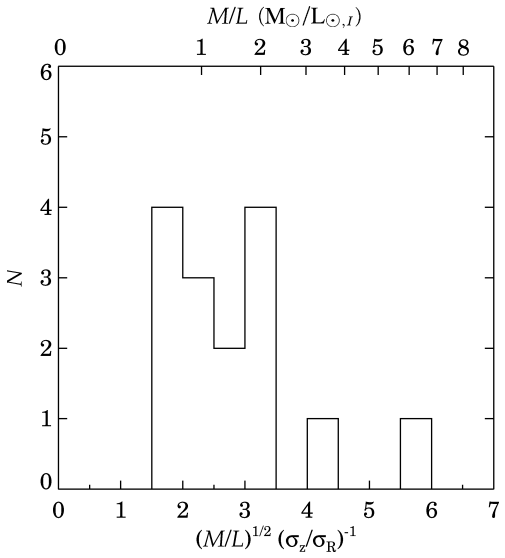

Figure 7. Histogram of the product $\sqrt{M/L}\,(\sigma_z/\sigma_R)^{-1}$. Except for two outliers, the distribution of $\sqrt{M/L}\,(\sigma_z/\sigma_R)^{-1}$ is rather narrow. Along the top we show the values of M/L implied by $\sigma_z/\sigma_R = 0.6$ and the 0.7 mag luminosity correction of Section 3.5.1.

massive discs show more pronounced spiral structure in agreement with their lower σ_z/σ_R.

Although a constant Q among late-type spirals is appealing, the contrary is certainly possible. For example, LSB spirals almost certainly have disc surface densities that are significantly lower than those of HSBs. In Section 3.3, evidence will be presented indicating that LSB discs have only slightly lower velocity dispersions. In that case, the Q parameter (equation 11) is expected to be larger for LSB discs. The data support such a behaviour when σ_z/σ_R is approximately constant (Fig. 6b). For $\sigma_z/\sigma_R = 0.6$, discs that appear close to maximal have Q slightly larger than unity, indicating that these discs are only marginally stable to local perturbations. Submaximal discs, on the other hand, have Q in the range 1.5–3 and appear to be quite stable. Perhaps the truth lies in between the cases of constant Q and constant σ_z/σ_R. Finally, note that for galaxies close to maximum disc, Fig. 6(b) implies that the velocity anisotropy cannot be much larger than 0.6 since otherwise we would have $v_{\rm disc}/v_{\rm max} > 1$ and $Q < 1$.

3.1.2 Disc mass-to-light ratio

The distribution of the product $\sqrt{M/L}\,(\sigma_z/\sigma_R)^{-1}$ obtained in Paper IV is shown in Fig. 7. Of the 15 discs, 13 have $1.8 \lesssim \sqrt{M/L}\,(\sigma_z/\sigma_R)^{-1} \lesssim 3.3$. The outliers are ESO 487-G02 and 564-G27. Their values may have been overestimated: for ESO 487-G02, the rotation curve is unknown and only two stellar data points are available; and for ESO 564-G27, the stellar kinematics may be affected by dust extinction (see Paper IV). Excluding these two outliers, the average is $\langle\sqrt{M/L}\,(\sigma_z/\sigma_R)^{-1}\rangle = 2.5 \pm 0.2$ with a 1σ scatter of 0.6 (including the outliers yields an average 2.7 ± 0.2 with a scatter of 0.7). The near-constancy of the product can be used with M/L based on stellar population synthesis models to estimate the velocity anisotropy. This estimate is however less robust than that based on Toomre's Q, because of the considerable uncertainty in the face-on surface brightness of edge-on spirals (Section 2.1).

The adopted vertical exponential luminosity distribution applies to the old stellar population. The M/L in the product $\sqrt{M/L}\,(\sigma_z/\sigma_R)^{-1}$ therefore refers to this population. Taking $M/L_I = 3.6$ for the old population (Worthey 1994, for a single-burst 12-Gyr-old population of solar metallicity and a Salpeter initial mass function) implies $\sigma_z/\sigma_R \simeq 0.7$. Alternatively, the product $\sqrt{M/L}\,(\sigma_z/\sigma_R)^{-1}$ can also be corrected using the 0.7 mag offset between the I-band Tully–Fisher relations of edge-on and face-on spirals (Section 3.5). The corrected value is $\sqrt{M/L}\,(\sigma_z/\sigma_R)^{-1} = 1.8$. This can be used with an estimate of M/L based on observed colours to infer σ_z/σ_R. For late-type spirals at one disc scalelength, $B - I = 1.7 \pm 0.2$ (de Jong 1996b). According to the stellar M/L versus colour relation of BJ01, the maximum-disc scaled stellar M/L for this colour range corresponds to $M/L_I = 1.1$–1.7, yielding $\sigma_z/\sigma_R = 0.6$–0.7. For lower stellar M/L ratios implied by a 'bottom-light' initial mass function (IMF), $M/L_I \simeq 0.8$ (Portinari, Sommer-Larsen & Tantalo 2004), the implied velocity anisotropy is about 0.5.

In summary, independent knowledge of both Q and the stellar M/L ratio in conjunction with the current data suggests that the velocity anisotropy is in the range 0.5–0.7. This is similar to the solar neighbourhood value (Dehnen & Binney 1998; Mignard 2000), and lower than most values measured in early-type spirals (Shapiro et al. 2003). In the following, $\sigma_z/\sigma_R = 0.6$ will be adopted, bearing in mind an uncertainty of 0.1. The M/L scale implied by $\sigma_z/\sigma_R = 0.6$ and the 0.7 mag luminosity correction of Section 3.5.1 was added to Fig. 7, and corresponds to an average $M/L_I = 1.2 \pm 0.2\,(1\sigma)\,{\rm M}_\odot/{\rm L}_{\odot,I}$. Note that this value of M/L is not robust, since it depends rather sensitively on the adopted anisotropy and the luminosity correction.

3.2 Submaximal discs?

In the present sample, the observed rotational velocity at $2.2\,h_R$ is close to the observed maximum rotational velocity, i.e. $v_{\rm c}(2.2\,h_R) \simeq v_{\rm max}$ (Paper III). Hence, the disc contribution to the rotation curve at $2.2\,h_R$, i.e. $v_{\rm disc}/v_{\rm c}(2.2\,h_R)$, can be parametrized by the ratio $v_{\rm disc}/v_{\rm max}$ (equation 9). This ratio is known up to a factor of σ_z/σ_R and is distance-independent. Fig. 8 shows this parameter for $\sigma_z/\sigma_R = 0.6$ as a function of (a) maximum rotational velocity and (b) face-on surface brightness. Even though the uncertainties on the individual points are large, most galaxy discs cannot provide the observed maximum rotation. The disc contribution to the observed maximum rotation is on average only $v_{\rm disc}/v_{\rm max} = 0.58 \pm 0.05$, with a 1σ scatter of 0.18. For ESO 487-G02 and 564-G27, the $\sqrt{M/L}\,(\sigma_z/\sigma_R)^{-1}$ values are high (see Paper IV). Excluding these outliers from the average yields $v_{\rm disc}/v_{\rm max} = 0.53 \pm 0.04$, with a $1\,\sigma$ scatter of 0.15. A maximal disc, on the other hand, will have a contribution only a bit lower than unity. A working definition is $v_{\rm disc}/v_{\rm max} = 0.85 \pm 0.10$ (Sackett 1997), lower than unity to allow a bulge contribution and to let dark haloes have a low-density core. Thus, at least for this sample, the average spiral has a submaximal disc. Note that equation (9) strictly applies to a razor-thin disc. For a disc with a flattening of $h_R/h_z \simeq 10$, the radial gravitational force is weaker, leading to a decrease of about 5 per cent in $v_{\rm disc}/v_{\rm max}$ (van der Kruit & Searle 1982). Taking the gravity of the gas layer and dark halo into account would yield a 10 per cent effect, also in this direction (see the discussion in Paper IV).

The submaximal disc result can be questioned on three grounds: via the value for σ_z/σ_R, the stellar kinematics, or the assumed vertical density distribution. The remaining systematic effects are probably unimportant (see Paper IV). The argument can then be turned around. In order for the average disc in the sample to be maximal, either (1) the velocity anisotropy must be about 0.9 (almost isotropic), or (2) the intrinsic velocity dispersions have been under-

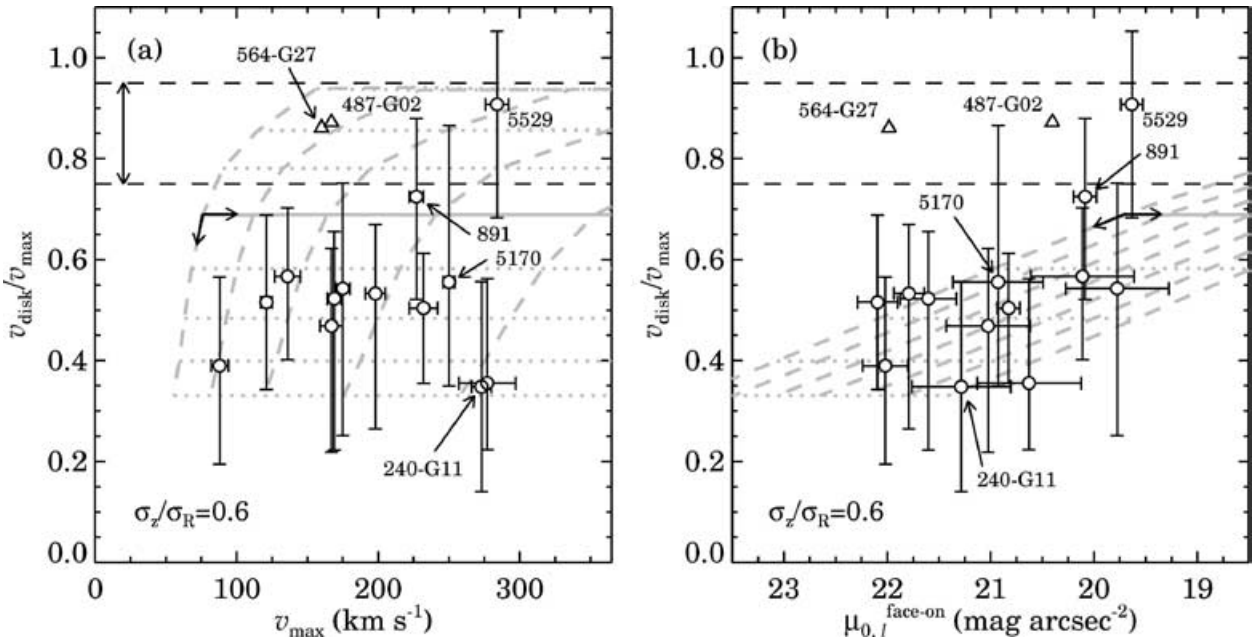

Figure 8. Contribution of the disc to the observed maximum rotation for $\sigma_z/\sigma_R = 0.6$: (a) as a function of maximum rotational velocity (circles) – the black dashed lines bracket the range for maximal discs (Sackett 1997); (b) as function of face-on central surface brightness. In both panels several galaxies are highlighted, and the triangles indicate the outliers in Fig. 7, ESO 487-G02 and 564-G27. The grey lines show the collapse model (DSS97 1997), the dashed lines connect models of the same total mass [$\log_{10}(M_{\rm tot}) = 10$–$13$ in steps of 0.5] and the dotted lines connect models with the same spin parameter (logarithmically spaced, separated by factors of 0.2 dex, with the solid line at $\lambda = 0.06$). The arrows indicate the direction of increasing $M_{\rm tot}$ and λ.

estimated by about 50 per cent (such that the average $v_{\rm disc}/v_{\rm max}$ is underestimated by 0.58/0.85), or (3) the vertical density distribution is more peaked than exponential at low z. Each of these three possibilities is very unlikely. A velocity anisotropy $\sigma_z/\sigma_R = 0.9$ would imply a stellar Q parameter below unity for half of the sample. In addition, such a velocity anisotropy cannot be attained according to the theory of disc heating (Jenkins & Binney 1990), and is even larger than the σ_z/σ_R measured in early-type spirals (Shapiro et al. 2003). In principle, the stellar kinematics may be affected by young stellar populations, which have a lower stellar velocity dispersion than the late-type stars that dominate the disc mass budget. However, the effect is only 20 per cent for a stellar composition resembling the solar neighbourhood (Fuchs 1999; van der Kruit 2001b). In addition, young populations were largely avoided by choosing edge-on spirals and placing the slit away from the plane. Finally, a density distribution that is more sharply peaked than exponential at $z \lesssim h_z$ would need to hide as much disc mass as is already contained in the exponential distribution. This appears to be unrealistic, especially considering that near the plane the observed vertical light distributions in the near-infrared (de Grijs, Peletier & van der Kruit 1997) still contain a small amount of light due to young red supergiants (Jones et al. 1981; Rhoads 1998). These stars make a very small contribution to the disc mass.

According to Fig. 8 the discs of five spirals may be close to maximal: ESO 487-G02 and 564-G27, and NGC 891, 5170 and 5529. However, for ESO 487-G02 and 564-G27 the $\sqrt{M/L}\,(\sigma_z/\sigma_R)^{-1}$ values are not solid. Taking, instead, the average $\sqrt{M/L}\,(\sigma_z/\sigma_R)^{-1}$ in the sample for these two galaxies would lower both of them to $v_{\rm disc}/v_{\rm max} \simeq 0.55$. While for NGC 891 and 5170 the most probable $v_{\rm disc}/v_{\rm max}$ are less than 0.75, the uncertainties allow a maximal disc according to the Sackett (1997) definition. The disc of the barred spiral NGC 5529 has a normal $\sqrt{M/L}\,(\sigma_z/\sigma_R)^{-1}$ combined with a high face-on surface brightness and a high radial velocity dispersion. It could be maximal, but the stellar and gas kinematics suggest that the disc is strongly perturbed and therefore the disc model may not be applicable. We note that the other two spirals in the sample for which there is kinematical evidence that they contain a bar are ESO 487-G02 and 240-G11 (Bureau & Freeman 1999; Paper III). Again, the value for ESO 487-G02 is uncertain. The disc of ESO 240-G11 is relatively flat (KKG), of low surface brightness and strongly submaximal.

This points to an important corollary. If the seven spirals with a boxy or peanut-shaped bulge (table 1 in Paper IV) are barred, then the submaximal nature of discs is not limited to normal spirals. Excluding ESO 487-G02 and 564-G27, the six spirals with a boxy or peanut-shaped bulge have on average $v_{\rm disc}/v_{\rm max} = 0.56 \pm 0.09$, with a 1σ scatter of 0.22. The seven remaining spirals, which do not have a boxy or peanut-shaped bulge, are practically indistinguishable, with an average $v_{\rm disc}/v_{\rm max} = 0.51 \pm 0.02$, and a 1σ scatter of 0.06. The association of boxy and peanut-shaped bulges with bars is well established (Kuijken & Merrifield 1995; Bureau & Freeman 1999). The results therefore suggest that at $2.2\,h_R$ the contribution of the disc to the rotation curve is independent of barredness. This is in agreement with the high-resolution N-body simulations by Valenzuela & Klypin (2003). These point out that discs can form bars even in the presence of strong haloes, and that these discs are submaximal at $2.2\,h_R$.

There is no clear evidence for an increase in $v_{\rm disc}/v_{\rm max}$ with $v_{\rm max}$ as suggested by Kranz et al. (2003). For example, the present sample contains three galaxies of high $v_{\rm max}$ (>200 km s^{-1}) that have submaximal discs: ESO 240-G11, 435-G25 and 437-G62. Excluding the values for ESO 487-G02 and 564-G27, there is perhaps a hint at a trend with surface brightness (Fig. 8b). However, the uncertainties are too large and the number of very high surface brightness discs is too small to address this properly. Similarly, there is no hard evidence for a trend of $v_{\rm disc}/v_{\rm max}$ with the total dynamical

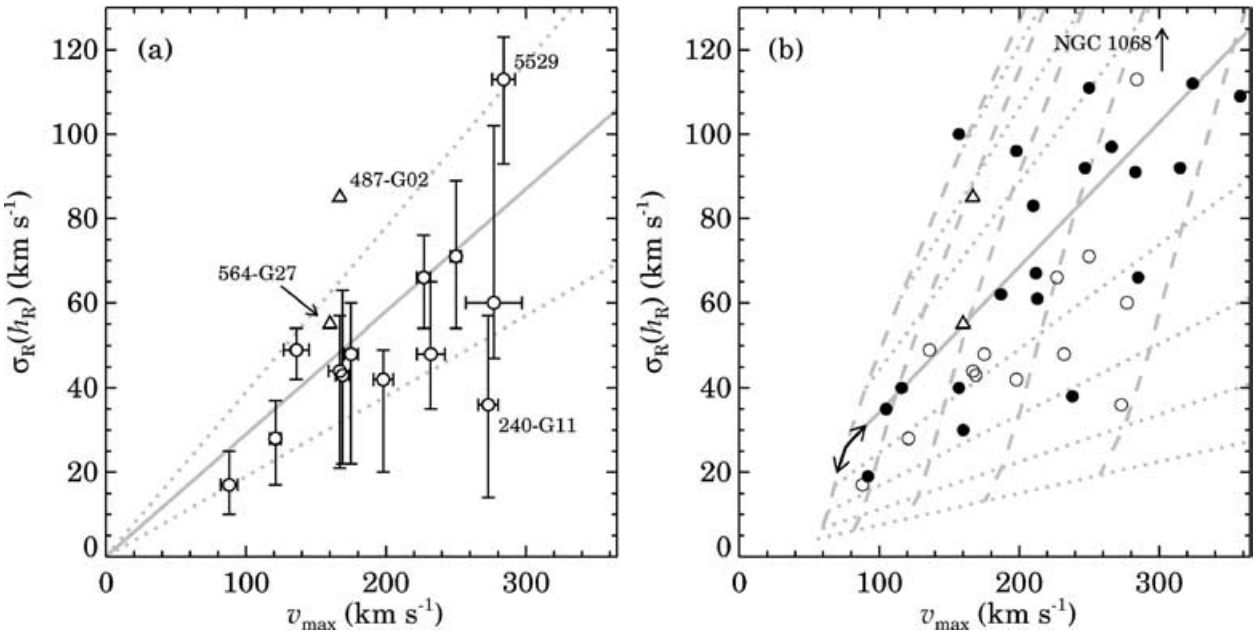

Figure 9. (a) Stellar disc velocity dispersion versus galaxy maximum rotational velocity. The grey lines indicate the relation $\sigma_R(h_R) = (0.29 \pm 0.10)\, v_{max}$ (B93). (b) Stellar disc velocity dispersion versus galaxy maximum rotational velocity for galaxies with published stellar velocity dispersions. Open circles and triangles indicate the present sample, filled dots the literature galaxies. Grey lines show the collapse model for $Q = 2.0$, as in Fig. 8. NGC 1068 lies outside the plotted region.

mass-to-light ratio (not shown). Note that the deprojected disc surface brightnesses (table 1 in Paper IV) strictly apply to the old disc light. The difference with the total integrated light is given attention in Section 3.5 and is found to be on average ∼0.7 mag.

The analytical collapse model of disc galaxy formation (Fall & Efstathiou 1980; Gunn 1982; DSS97) gives v_{disc}/v_{max} as a function of the total mass and spin parameter of the initial protogalaxy. To quantify this, model surface density profiles and rotation curves were calculated using the method of DSS97 for a range in spin parameter and total mass of the protogalaxy, taking a baryonic mass fraction $F = 0.10$ and a mass-to-light ratio $(M/L)_{disc} = 2$ (see Section 2.1 for details). The v_{disc}/v_{max} were calculated using equation (9), but taking the circular velocities at $2.2\, h_R$ instead of the maxima.

The result is shown in Fig. 8 (grey lines). In this picture the disc contribution increases with decreasing λ: more compact, higher surface density discs result from the collapse of lower-λ protogalaxies. An important feature of the model is that at constant λ the disc contribution is independent of M_{tot} (v_{max}), because the disc rotation and the maximum rotation both increase as $M_{tot}^{1/3}$. Since DSS97 have shown that the collapse model roughly matches the observed distribution of disc central surface brightness and scalelength, it comes as no surprise that the range of inferred v_{disc}/v_{max} corresponds to the observed range. Interestingly, the model predicts a gradual increase in the disc contribution towards higher surface brightness discs, not inconsistent with the data (Fig. 8b). The model trends are independent of the adopted baryonic mass fraction and M/L, and are in qualitative agreement with more detailed semi-numerical disc galaxy formation models (e.g. Zavala et al. 2003). These trends actually follow from several well-known arguments, as will be discussed in Section 3.4.

3.3 The σ versus v_{max} relation

Observations of the stellar kinematics in 11 HSB spirals by B93 have revealed a related trend: more rapidly rotating spirals appear to have larger stellar velocity dispersions. Fig. 9(a) shows the stellar disc velocity dispersion $\langle \sigma_R(h_R) \rangle_z$ versus the galaxy maximum rotational velocity. A Spearman rank correlation test yields a correlation coefficient $R_S = 0.44$, or a confidence level of 90 per cent (about 2σ). The confidence level is somewhat low, mainly due to ESO 240-G11. This spiral will be discussed below. An ordinary linear least-squares fit to the data yields a slope of 0.22 ± 0.10 and an intercept 10 ± 17 km s^{-1}. The scatter about this relation is 22 km s^{-1} (1σ) in σ_R. The correlation is similar to that reported by B93 (grey lines), although the samples have NGC 891 and 5170 in common. A simple linear least-squares fit, adopted from his fig. 6, gives

$$\sigma_z|_{R=0} = (0.29 \pm 0.10) v_{max}. \quad (12)$$

The present study improves upon the statistics of the σ versus v_{max} relation, almost doubling the total number of spiral galaxies with known stellar disc velocity dispersions. The spirals with previously published velocity dispersions are gathered in Table 2, and the distribution of the combined sample in the σ versus v_{max} plane is shown in Fig. 9(b). A Spearman rank correlation test applied to the combined sample of 36 galaxies yields $R_S = 0.68$, or a confidence level greater than 99 per cent. An ordinary linear least-squares fit yields a slope of 0.33 ± 0.05 and an intercept -2 ± 10 km s^{-1}. The scatter about this linear relation is 25 km s^{-1} (1σ). This slope and intercept are in agreement with the simple linear relation $\sigma_R(h_R) = 0.29\ v_{max}$, which, to be consistent with KKG, will be adopted as the average σ versus v_{max} relation in the remainder of this paper. The Sb Seyfert NGC 1068 and the S0a NGC 6340 lie far above the average relation. NGC 6340 is the only early-type disc galaxy in the B93 sample. Note that in B93 the maximum rotation of NGC 6340 was erroneously assigned too high a value, causing it to lie closer to the mean relation. The lower value $v_{max} = 157$ km s^{-1} implied by the *HST* Key Project Tully–Fisher relation (Sakai et al. 2000) fits better with its small scalelength $h_{R,B} = 2.7$ kpc (cf. Fig. 1).

Table 2. Galaxies with published stellar disc velocity dispersions.

Galaxy	Type	$v_{\rm max}$ (km s^{-1})	$\sigma_R(h_R)$ (km s^{-1})	h_R (arcsec)	Ref.	Notes
(1)	(2)	(3)	(4)	(5)	(6)	(7)
Milky Way	SABbc	210 ± 25	83 ± 24	3 ± 1 kpc	a	
NGC 488	Sb	358 ± 16	109 ± 32	32	b	iii
NGC 1068	Sb	302 ± 44	159 ± 20	21	b	iii
NGC 1566	SBbc	212 ± 30	$67 \pm ^{26}_{14}$	35	c	ii
NGC 2460	Sab	198 ± 24	96 ± 12	15	b	iii
NGC 2552	SBm	92 ± 3	19 ± 2	33	d	iv, v
NGC 2613	Sb	315 ± 10	92 ± 32	–	c	
NGC 2775	Sab	283 ± 4	91 ± 14	35	b	iii
NGC 2815	SBb	285 ± 5	66 ± 12	46	c	
NGC 2985	Sab	250 ± 15	111 ± 12	30	b	iii
NGC 2998	SBc	213 ± 8	61 ± 15	17	e	
NGC 3198	SBc	157 ± 2	40 ± 7	58	c	
NGC 3938	Sc	160 ± 20	30 ± 8	36	c	ii, iv
NGC 4030	Sbc	247 ± 51	92 ± 23	18	b	iii
NGC 5247	SBbc	187 ± 20	40 ± 62	10	f	ii, iv
NGC 6340	S0-a	157 ± 40	100 ± 20	25	c	ii, iv
NGC 6503	Sc	120 ± 2	33 ± 4	24	c	
NGC 7184	SBbc	266 ± 10	96 ± 25	48	c	
NGC 7331	Sbc	257 ± 5	38 ± 11	52	g	
NGC 7782	Sb	324 ± 24	112 ± 50	22	h	i, iv, v
IC 5249	Scd	105 ± 5	35 ± 5	40	i	

(1) Galaxy. (2) Morphological type. (3) Maximum rotational velocity. (4) Radial velocity dispersion at one scalelength. (5) Disc scalelength (photometric). (6) References: (a) Lewis & Freeman (1989), (b) Shapiro et al. (2003), (c) B93, (d) Swaters (1999), (e) Swaters, Bottema & Kregel (in preparation), (f) van der Kruit & Freeman (1986), (g) Bottema (1999), (h) Pignatelli et al. (2001), (i) van der Kruit et al. (2001). (7) Additional notes: (i) maximum rotational velocity taken from LEDA; (ii) maximum rotational velocity according to the *I*-band Tully–Fisher relation of Sakai et al. (2000) using the extinction corrected magnitudes from LEDA; (iii) taking for $v_{\rm max}$ the value of their parametrized rotation curve at $2.2\,h_R$; (iv) assuming $\sigma_z/\sigma_R = 0.6$ (see B93); (v) assuming $\sigma_\phi = \sigma_z$.

When combined with the Toomre criterion (equation 11), the collapse model for disc galaxy formation (DSS97) gives the velocity dispersion. This is shown in Fig. 9(b) for $Q = 2.0$, again for lines of constant $M_{\rm tot}$ and λ. For constant Q the collapse model predicts galaxy discs to be distributed in a large portion of the σ versus $v_{\rm max}$ plane. Discs originating from haloes with the same λ occupy straight lines of slope $\sigma/v_{\rm max}$; at constant λ local stability requires that the discs of more massive spirals have a larger velocity dispersion. This suggests that the correlation between σ_R and $v_{\rm max}$ is a result of local stability (B93; Boissier et al. 2003; van der Kruit 1995). Model discs residing in haloes with a higher-than-average spin parameter have lower surface densities and lower $v_{\rm disc}/v_{\rm max}$ (cf. Fig. 8). If Q is constant, then these model discs also have lower velocity dispersions. Hence, for constant Q the collapse model suggests that discs do not define a single linear relation in Fig. 9. For a peaked distribution of halo spin parameters, the model discs scatter about a linear σ versus $v_{\rm max}$ relation, with a slope corresponding to the average λ and a scatter related to the spread in λ. Adopting a different baryonic fraction does not change the trend.

For the Q implied by a constant σ_z/σ_R (Fig. 6b), the portion of the σ versus $v_{\rm max}$ plane occupied by the collapse model narrows considerably. In fact, for a form $Q \propto (v_{\rm disc}/v_{\rm max})^{-2}$, the model discs all follow a single straight line. The particular example shown in Fig. 6(b) (dotted line) gives a relation $\sigma_R(h_R) = 0.29\,v_{\rm max}$. However, the correlation between the disc flattening and the total dynamical mass-to-light ratio $M_{\rm dyn}/L_{\rm disc}$ (cf. Section 2.1) does indicate that there is at least one other parameter in the σ versus $v_{\rm max}$ relation. For the power-law relation fitted to the observed relation between h_R/h_z and $M_{\rm dyn}/L_{\rm disc}$ (equation 10),

$$\begin{aligned}\frac{\sigma_R}{v_{\rm max}} &\propto \left(\frac{\sigma_z}{\sigma_R}\right)^{-1}\left(\frac{h_R}{h_z}\right)^{-1.17}\left(\frac{M}{L}\right)^{1/2}_{\rm disc}\\ &\propto \left(\frac{\sigma_z}{\sigma_R}\right)^{-1}(\mu_0)^{0.44}\left(\frac{M}{L}\right)^{1/2}_{\rm disc}\\ &\propto \left(\frac{\sigma_z}{\sigma_R}\right)^{-1}\left(\frac{M_{\rm dyn}}{L_{\rm disc}}\right)^{-0.88}\left(\frac{M}{L}\right)^{1/2}_{\rm disc},\end{aligned} \tag{13}$$

which varies among discs unless the right-hand products are all constant. The latter is unlikely, even though the anisotropy is roughly constant (Section 3.1). For example, for the first equation there is evidence that the flattening increases (Fig. 1f) and the disc M/L ratio decreases (BJ01) towards lower surface brightness.

The scatter on the σ versus $v_{\rm max}$ relation is comparable to the uncertainties (Fig. 9a), providing no evidence in itself for another parameter. It was therefore investigated whether the deviations from the average relation $\sigma_R^{\rm avg} = 0.29 v_{\rm max}$ correlate with any of the parameters of equation (13). In Fig. 10 this scatter is shown versus disc flattening, face-on central surface brightness and dynamical mass-to-light ratio. Although the uncertainties are large, a Spearman rank test provides evidence for a negative correlation in each case (at the 1.3σ, 2.1σ and 1.6σ levels, respectively). Hence, the σ versus $v_{\rm max}$ relation is probably not a single linear relation. Discs with a smaller radial stellar velocity dispersion tend to be more flattened, and have a lower surface brightness and a higher dynamical mass-to-light ratio. Note that ESO 487-G02 and 564-G27, the two outliers in Fig. 7, are also outliers in Figs 10(b) and (c).

3.4 Implications for models of disc formation

We have found that the collapse model of DSS97 provides good fits to our distributions. However, this does not imply that this model has all the correct features and mechanisms for disc formation. Many of the model trends follow from simple arguments that are independent of the actual manner in which discs have formed. We will illustrate this here.

The linear σ versus $v_{\rm max}$ relation follows from straightforward arguments (van der Kruit 1990; B93; van der Kruit & de Grijs 1999). Below we will always evaluate all properties at one radial scalelength ($R = 1\,h_R$) without using subscripts to indicate this. Using the definition for Toomre Q in equation (11) for a flat rotation curve, so that $\kappa = \sqrt{2}\,v_{\rm max}/R$, and eliminating h_R using a Tully–Fisher relation $L_{\rm disc} \propto \mu_0 h_R^2 \propto v_{\rm max}^4$ results in

$$\sigma_R \propto Q\frac{\mu_0 (M/L)_{\rm disc} h_R}{v_{\rm max}} \propto Q\left(\frac{M}{L}\right)_{\rm disc}\mu_0^{1/2} v_{\rm max}. \tag{14}$$

This shows that, when Q and M/L are constant among galaxies, galaxy discs with lower (face-on) central surface brightness μ_0 have lower stellar velocity dispersions (Fig. 10b). Combining equation (14) with hydrodynamic equilibrium (equation 3) gives

$$\frac{h_R}{h_z} \propto Q\left(\frac{\sigma_R}{\sigma_z}\right)\sigma_z^{-1} v_{\rm max}. \tag{15}$$

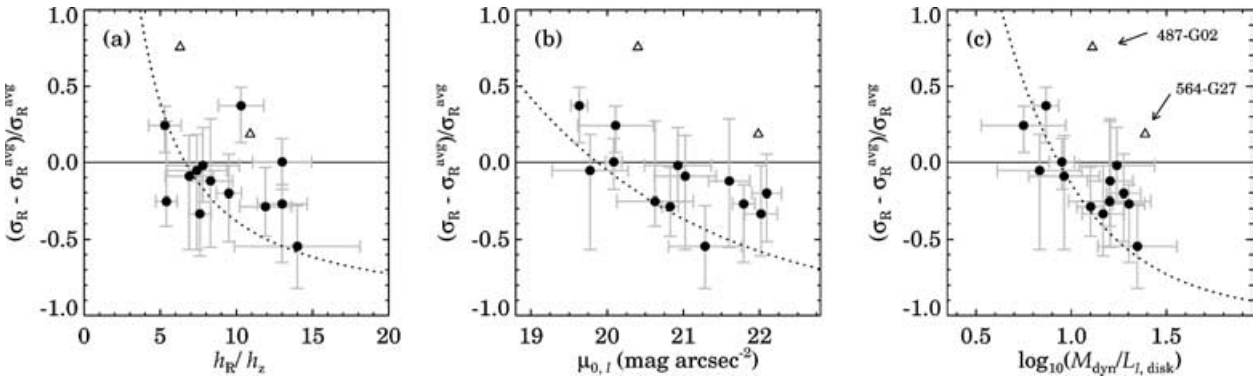

Figure 10. Deviation from the average σ versus v_{max} relation as a function of (a) intrinsic disc flattening, (b) I-band face-on central surface brightness, and (c) dynamical mass-to-light ratio. The dotted lines indicate equation (13), arbitrarily shifted in zero-point roughly to match the data. The two outliers are indicated.

This is equivalent to equation (16) in van der Kruit & de Grijs (1999). It can also be written as

$$\sigma_z \propto Q \left(\frac{h_R}{h_z}\right)^{-1} \left(\frac{\sigma_R}{\sigma_z}\right) v_{\rm max}. \tag{16}$$

Apart from the exponent of the flattening (-1 versus -1.17), this is the same as equation (10) in the case that $\sqrt{M/L}\,(\sigma_R/\sigma_z)^{-1}$ is constant (as in Fig. 7). Note, however, that equation (10) was derived from the observed correlation between the flattening h_R/h_z and the ratio of the dynamical mass $M_{\rm dyn} = 4h_R v_{\rm max}^2/G$ to the total disc luminosity $L_{\rm disc}$. Using μ_0 from equation (3) and $v_{\rm max}$ from equation (15),

$$\frac{M_{\rm dyn}}{L_{\rm disc}} \propto \left(\frac{h_R}{h_z}\right) \left(\frac{\sigma_R}{\sigma_z}\right)^{-2} Q^{-1} \left(\frac{M}{L}\right)_{\rm disc}. \tag{17}$$

This is consistent with that fit apart from the exponent of $M_{\rm dyn}/L_{\rm disc}$, which was 0.75 ± 0.11 in the observations. Equation (15) combined with equations (2) and (14) gives

$$\frac{v_{\rm disc}}{v_{\rm max}} = Q \left(\frac{M}{L}\right) \mu_0^{1/2} \left(\frac{\sigma_R}{\sigma_z}\right)^{-1} \left(\frac{h_R}{h_z}\right)^{1/2}. \tag{18}$$

Combining equations (14) and (16) we find the velocity anisotropy

$$\left(\frac{\sigma_R}{\sigma_z}\right)^2 \propto \left(\frac{M}{L}\right)_{\rm disc} \mu_0^{1/2} \left(\frac{h_R}{h_z}\right)^{-1}, \tag{19}$$

which is the equivalent of equation (17) in van der Kruit & de Grijs (1999), except for the inclusion of μ_0. Finally we combine equations (15) and (14) and find for the flattening

$$\frac{h_R}{h_z} \propto \left(\frac{\sigma_R}{\sigma_z}\right)^2 \left(\frac{M}{L}\right)_{\rm disc}^{-1} \mu_0^{-1/2}. \tag{20}$$

This shows that low surface brightness galaxies tend to be flatter (Fig. 1f).

Note that we repeatedly see the combination $\sqrt{M/L}\,(\sigma_R/\sigma_z)^{-1}$ in the equations. When this product (or of course M/L and σ_R/σ_z separately) and Q are constant among galaxies (as Fig. 7 indicates), many of the observed correlations result. So we conclude that indeed there is little variation of these properties among galaxy discs. We already noted that equation (14) resembles the observed trend in Fig. 10(b). The correlation of the flattening with the ratio of dynamical mass to disc luminosity in equation (17) and with surface brightness in equation (20) correspond to Figs 10(b) and (c).

This illustration shows that the observed trends follow from first principles without detailed assumptions on the details of the formation of discs, as long as actual mechanisms working during galaxy formation ensure that the Toomre parameter Q and the combination $\sqrt{M/L}\,(\sigma_R/\sigma_z)^{-1}$ are approximately constant among galaxies (such mechanisms are not included in the collapse model of DSS97). Stellar discs of galaxies then become essentially a two-parameter family. Disc size (or scalelength) and disc luminosity (or equivalently surface brightness) determine the basic structure. The Tully–Fisher relation then prescribes what the rotation velocity should be. It is the scatter in Q and $\sqrt{M/L}\,(\sigma_R/\sigma_z)^{-1}$ that is responsible for the scatter in the flattening (equation 19 or 20), in the disc contribution to the rotation curve (equation 18) and in $M_{\rm dyn}/L_{\rm disc}$ (equation 17) of discs of otherwise similar size and luminosity. The variation of the properties of galaxy discs, both structural (the scale parameters and flattening as a function of surface brightness, rotation velocity and dynamical mass-to-light ratio) as well as kinematical (disc contribution to the rotation and velocity dispersion as a function of surface brightness and rotation velocity) follow quite naturally from collapse models (DSS97), with a range of total masses of 10^{10}–10^{13} $M_\odot$ and spin parameter λ in the range 0.06–0.20.

3.5 The Tully–Fisher relation

In recent years, studies on the nature of the Tully–Fisher (TF) relation have started to focus on the baryonic mass TF relation, i.e. the relation between stellar plus gaseous mass and the maximum rotational velocity (McGaugh et al. 2000; BJ01). One of the ultimate goals is to use the observed baryonic mass TF relation to constrain models of hierarchical structure formation. These studies start at the classic luminosity TF relation and use stellar population synthesis models to estimate the stellar mass TF relation of galaxy discs. The stellar mass TF is then combined with estimates of the gaseous mass to arrive at the baryonic mass TF relation. Edge-on spirals cannot provide direct information regarding the classic luminosity TF relation because of a large and uncertain effect of dust extinction (Paper II). We encountered a similar situation regarding the disc mass-to-light ratio in Section 3.1 (see also Paper IV). Their observed stellar kinematics do pin down the stellar disc masses, thereby providing a dynamical route to the stellar and baryonic mass TF relations.

3.5.1 The luminosity TF relation for edge-on spirals

The luminosity TF relation can be compared to the now well-known relation for less inclined spirals (Sakai et al. 2000; Verheijen 2001) to gain insight into the nature of the missing light in edge-on spirals. For the rotation, the maximum rotational velocity was taken (table 1 in Paper IV). For the luminosity, the I-band values of the best-fitting 2D models have been used (KKG; for NGC 5170, see Paper I; for

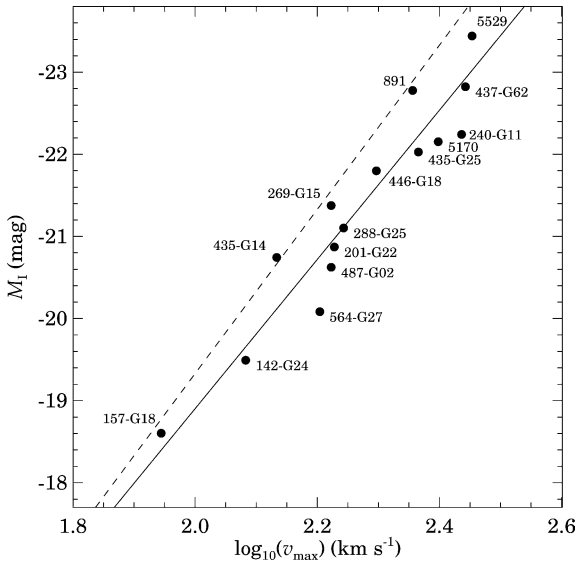

Figure 11. The *I*-band Tully–Fisher relation, using the model luminosities and the observed maximum rotational velocities. The solid line indicates a least-squares bisector fit to the data. The dashed line indicates the *I*-band TF of the *HST* Key Project (Sakai et al. 2000).

ESO 435-G25, and NGC 891 and 5529, see Xilouris et al. 1999). These model luminosities minimize the effect of dust extinction, which is clearly present in the purely observational luminosity–linewidth relation (Paper II). Considering the model luminosities also allows a check on the amount of light still missing in the deprojected surface brightnesses (table 1 in Paper IV), which only take into account the old disc population. For the eight galaxies with a clear bulge, namely the galaxies with $\log_{10}(v_{\rm max}) > 2.3$ plus ESO 487-G02, the luminosities include the bulge luminosity. For the remaining systems, a bulge is either not present or too compact to be modelled (KKG). For these small, late-type spirals, the bulge luminosities are probably less than 20 per cent of the disc luminosities (de Jong 1996a). The luminosities were also corrected for the radial truncation, if detected. For this correction, the truncation radii $R_{\rm max}$ from table 5 in KKG and the literature were used (NGC 891 from van der Kruit & Searle 1981; ESO 435-G25 and NGC 5170 from Pohlen, Dettmar & Lütticke 2000), and it was assumed that the truncation is infinitely sharp (i.e. zero luminosity density at radii larger than $R_{\rm max}$). The average correction is 9 per cent of the disc luminosity. Finally, the luminosities were corrected for Galactic extinction using the values of table 1 in Paper IV.

Fig. 11 shows the TF relation, scaled to $H_0 = 71$ km s^{-1} Mpc^{-1} (Sakai et al. 2000). The solid line shows an unweighted least-squares bisector fit to the data. It has a slope[3] $\alpha = 3.64 \pm 0.26$ and an intercept $\log_{10}(L_{100}/{\rm L}_\odot) = 9.22 \pm 0.07$. The *I*-band TF relation as determined by the *HST* Key Project (Sakai et al. 2000, their equation 11) is shown by the dashed line. Sakai et al. (2000) used the H I linewidth at the 50 per cent level ($W_{R,50}$). For regular spirals $W_{R,50}/2$ is a good approximation to the maximum rotational velocity (Verheijen 2001). For example, for the 11 spirals in common with Paper II, the difference between the two values ($v_{\rm max} - W_{R,50}/2$) is on average -2.5 km s^{-1} with a 1σ scatter of 4.3 km s^{-1}. The *HST* Key Project luminosities were corrected for extinction to the face-on orientation using the Tully et al. (1998) scheme.

[3] See footnote 2.

Considering that the sample size is small, the slope of the 'edge-on TF relation' is consistent with the *HST* Key Project slope ($\alpha = 4.00 \pm 0.04$). The edge-on TF does lie systematically below the 'face-on TF', as expected. The offset is about 0.7 mag (or about 0.08 dex in velocity). These 0.7 mag were used in Section 3.1.2 to correct the product $\sqrt{M/L}\,(\sigma_z/\sigma_R)^{-1}$ and estimate the velocity anisotropy. The offset cannot be explained as being due to distance errors in the present sample (0.1 mag for a systematic distance error of 5 per cent) or due the uncertainty in the zero-point of the face-on TF, which is only 0.13 mag (Sakai et al. 2000). Instead, most of the offset is probably caused by the following effects.

First, the vertical exponential disc model refers to the old stellar populations and does not take into account the (mostly obscured) light from young stellar populations in the galaxy plane (Paper IV). The fraction of the disc light arising from young stellar populations in the *I*-band may be estimated using stellar population synthesis models. For example, in order to match the observed integrated colours of late-type spirals, $B - I = 1.4$–2.0 (de Jong 1996b), the Worthey (1994) model suggests that for a constant star formation rate and solar metallicity roughly 30 per cent of the *I*-band luminosity is due to young stars (ages less than 1 Gyr). Secondly, while care was taken in the 2D modelling to exclude the region affected by dust extinction (KKG), it is possible that a small amount of extinction still plays a role at large z heights. Especially in large spirals ($\log_{10}(v_{\rm max}) \gtrsim 2.3$) dust features are often present at distances greater than 400 pc from the plane (Howk & Savage 1999). Extraplanar dust extinction probably has a smaller effect on the observed luminosities of less massive spirals. However, the offset between the edge-on and face-on TF relations appears similar for both large and small systems. This suggests, although the number of spirals at low $v_{\rm max}$ is small, that extinction can only explain part of the observed offset. A final possibility is that the disc model underestimates the old disc luminosity density at $|z| \leqslant 1.5\,h_z$. This would require a vertical luminosity distribution of old stars that is more sharply peaked than exponential, which is unlikely (de Grijs et al. 1997).

Finally, note that for a vertical light distribution shallower than exponential the inferred model luminosities would have been smaller. For example, for an isothermal distribution the old disc luminosity would be reduced by a factor of 2, causing the offset with the face-on TF relation to increase to about 1.5 mag. In that case it appears unlikely that the offset can be explained by young populations and residual dust extinction, implying that the isothermal is indeed not an adequate description for the old disc light.

3.5.2 The stellar disc mass TF relation

The stellar disc masses were calculated using $M_\star = 2\pi h_R^2 \Sigma_0$ and assuming $\sigma_z/\sigma_R = 0.6$. These masses were then refined by applying two corrections. First, the disc masses were corrected for the radial truncation, as in the above for the disc luminosities. Secondly, it will be recognized here that the neglect of the gas gravity has led to a slight overestimate of the stellar disc surface densities (Paper IV). The adopted correction factors are listed in table C2 in Paper IV. The effect of the neglect of the halo gravity is similar (Paper IV) but cannot be estimated reliably for individual cases. It should be kept in mind that on average the disc masses are probably overestimated by about 10 per cent.

Another effect that may be present is a decline of the stellar M/L with galactocentric radius, as suggested by the bluer broad-band colours at larger radii (de Jong 1996b; Bell & de Jong 2000). The M/L obtained by fitting the constant M/L model is then essentially

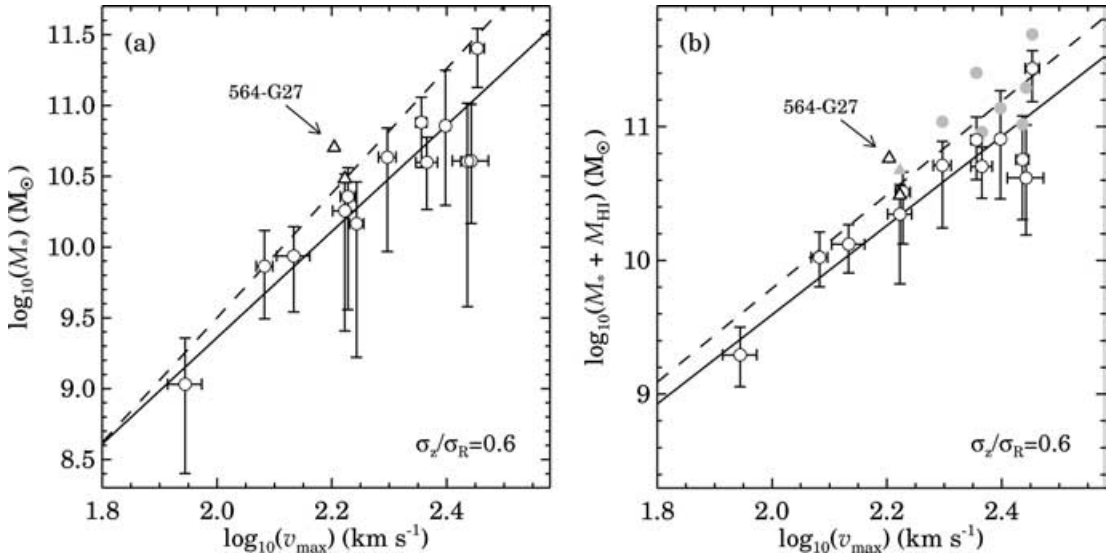

Figure 12. (a) The stellar disc mass TF relation, assuming $\sigma_z/\sigma_R = 0.6$. The solid line indicates the least-squares bisector fit. The dashed line represents the bisector fit to the maximum-disc scaled stellar mass TF relation of the Ursa Major cluster (BJ01). Triangles indicate the outliers in Fig. 7, ESO 487-G02 and 564-G27. (b) The baryonic mass TF relation after adding the observed H I mass. Triangles are as in (a). The solid line indicates a least-squares bisector fit, and the dashed line represents the bisector fit to baryonic mass TF relation of the Ursa Major cluster (BJ01). The grey dots include an uncertain estimate for the bulge mass (see text).

the average M/L in the inner, fitted region (see Paper IV). However, when this M/L is extrapolated to apply for the entire disc the actual stellar disc mass will be overestimated. An estimate of this possible effect was obtained assuming that the M/L ratio declines exponentially,

$$\frac{M}{L} = \frac{\Sigma_0\, \mathrm{e}^{-R/h_{R,M}}}{\mu_0\, \mathrm{e}^{-R/h_{R,L}}} = \left(\frac{M}{L}\right)_0 \mathrm{e}^{-R/h_{R,M/L}}, \qquad (21)$$

and using the median I-band to K-band scalelength ratio $h_R^I/h_R^K = 1.12$ (de Grijs 1998) for the ratio of the luminosity and mass scalelengths $h_{R,L}/h_{R,M}$. Such a declining M/L has a large scalelength $\sim 8\, h_R^I$, causing the total stellar mass to be about 10 per cent smaller than in the constant M/L case. It was chosen not to include this correction because it cannot be estimated reliably for an individual galaxy.

Fig. 12(a) shows the resulting stellar disc mass–rotational velocity relation, assuming a velocity anisotropy $\sigma_z/\sigma_R = 0.6$. The solid line shows an unweighted least-squares bisector fit to the data (excluding ESO 487-G02 and 564-G27). It has a slope[4] $\alpha = 3.75 \pm 0.40$ and an intercept $\log_{10}(M_{100}/\mathrm{M}_\odot) = 9.36 \pm 0.08$. The observed scatter around this relation is 0.22 dex in mass. An interesting comparison can be performed with the stellar mass TF of the Ursa Major cluster (BJ01). BJ01 pointed out that stellar population synthesis models show a tight correlation between stellar M/L and colour provided that the spiral galaxy IMF is universal. They calibrated the predicted stellar M/L using the observed K-band maximum-disc stellar M/L versus $B - R$ colour relation of the Ursa Major cluster sample of Verheijen (1997), and used it to convert the observed luminosities to stellar masses. They used the Tully et al. (1998) scheme to correct for extinction, and adopted the *HST* Key Project value of 20.7 Mpc for the distance to Ursa Major. The least-squares bisector fit to their maximum-disc scaled stellar mass TF relation is reproduced in Fig. 12(a) (dashed line). Since the Ursa Major cluster consists mainly of late-type galaxies having insignificant bulges, this stellar mass TF is essentially a stellar disc mass TF and may be compared to the present results.

The slope of the dynamical disc mass TF for the present sample is marginally consistent with that of the maximum-disc scaled stellar mass TF of BJ01 for which

$$\alpha = 4.4 \pm 0.2\,(\mathrm{random}) \pm 0.2\,(\mathrm{systematic}).$$

An exact match of the slopes is, however, not expected considering the small sample sizes. For example, the slope of the dynamical mass TF depends rather sensitively on the inclusion of the dwarf galaxy ESO 157-G18 ($\log_{10} v_{max} = 1.944$). More intriguing is the difference in intercept; the dynamically determined disc masses of the present sample are on average about 0.32 dex smaller than the maximum-disc scaled disc masses of the Ursa Major spirals (a disagreement of 2σ). The only spiral that lies above the maximum-disc scaled stellar mass TF is ESO 564-G27. Again, for ESO 564-G27 the $\sqrt{M/L}\,(\sigma_z/\sigma_R)^{-1}$ value is high and it was therefore excluded from the fit. Note that if the corrections for a declining M/L and the dark halo gravity discussed above were applied, this offset would grow to -0.40 dex.

What could explain the observed offset between the dynamical disc mass TF and the maximum-disc scaled stellar mass TF? BJ01 quote a distance uncertainty of 15 per cent corresponding to an uncertainty of 0.06 dex in the TF intercept. Allowing for a similar uncertainty in the present sample makes it clear that the offset between the two relations cannot be entirely ascribed to distance errors. BJ01 use the rotational velocities on the flat part of the rotation curve (v_{flat}), whereas for the dynamical mass TF the v_{max} are used. In the present sample only ESO 240-G11, 435-G14 and 564-G27 have $v_{max} > v_{flat}$ (Paper III). Using the v_{flat} for these galaxies still gives an offset in Fig. 12(a) of 0.24 dex. There is an uncertainty in the extinction correction; BJ01 demonstrate that using the (Tully & Fouque 1985) scheme instead of the Tully et al. (1998) corrections reduces the zero-point of the maximum-disc scaled stellar mass TF by -0.13 dex. This is also too small to explain the observed offset.

[4] $M/\mathrm{M}_\odot = (M_{100}/\mathrm{M}_\odot)\,[v_{max}/(100\,\mathrm{km\,s^{-1}})]^\alpha$.

How much of an offset would be expected if the Ursa Major spirals instead have submaximal discs? Using the average observed disc contribution in the present sample $v_{\rm disc}/v_{\rm max} = 0.53$ (Section 3.2) and taking $v_{\rm disc}/v_{\rm max} = 0.85$ for a maximal disc (Sackett 1997), the ratio of the submaximal stellar disc mass to the maximal stellar disc mass is 0.39, corresponding to 0.41 dex. This is able to explain the observed offset; the two relations practically coincide when the Ursa Major spirals, like most of the spirals in the present sample, have submaximal discs.

This has two important implications. First, submaximal discs require that the true stellar disc M/L ratios are a factor of 2 lower than the maximum-disc scaled M/L. This can be achieved by lowering the fraction of stars at the low-mass end of the IMF ($M < 0.5\,{\rm M}_{\odot}$). Such a 'bottom-light' IMF is supported by recent independent determinations in the solar neighbourhood (Kroupa 2002) and implies stellar M/L ratios for late-type spirals of $M/L_I \simeq 0.8$ (Portinari et al. 2004). In turn, there is little room in the disc for forms of matter other than stars and H I gas, such as dark matter or cold molecular gas. Any significant additional component would require an even lower stellar M/L.

3.5.3 The baryonic disc mass TF relation

The H I masses of all of the spirals except ESO 288-G25 are known (Paper I). Hence, the baryonic mass TF relation can also be investigated, modulo the uncertain molecular gas mass and the bulge contribution. To be consistent with BJ01, the H I masses were *not* corrected for helium and metals. The baryonic TF relation obtained after adding the H I mass to the dynamical stellar disc masses is shown in Fig. 12(b) (again using $H_0 = 71$ km s^{-1} Mpc^{-1}). An unweighted least-squares bisector fit to the data yields a slope $\alpha = 3.33 \pm 0.37$ and an intercept $\log_{10}(M_{100}/{\rm M}_{\odot}) = 9.59 \pm 0.07$. The observed scatter is 0.21 dex in mass. The shallower slope of the baryonic mass TF compared to the stellar mass TF is a result of the larger gas fraction in less massive galaxies. If the H I masses are corrected for helium and metals using $M_{\rm gas} = 1.4\,M_{\rm HI}$, then a fit yields $\alpha = 3.23 \pm 0.36$ and $\log_{10}(M_{100}/{\rm M}_{\odot}) = 9.66 \pm 0.07$ (not shown). Again, the maximum-disc scaled baryonic TF of BJ01 is shown for comparison [dashed line, slope $\alpha = 3.5 \pm 0.2$ (random) $\pm$ 0.2 (systematic)]. The dynamically determined baryonic TF is offset from the maximum-disc scaled stellar mass TF by about -0.24 dex, a similar offset as seen for the stellar mass TF. The present approach does not allow a study of the full stellar mass and baryonic mass Tully–Fisher relations; a comparison with, for example, predictions from cold dark matter simulations (Bullock et al. 2001b) would need a bulge dynamical mass estimate. However, inclusion of the bulge masses is expected to steepen the observed slope significantly. For example, Fig. 12(b) (grey symbols) shows the result after inclusion of an estimated bulge mass, derived from the bulge luminosities (table 3 in KKG; and Xilouris et al. (1999) for ESO 435-G25, and NGC 891 and 5529) using a bulge M/L_I of 5.5 (Bottema 1999). For those galaxies for which we have no reliable estimate of the bulge luminosity, the bulges are small and the contributions probably negligible. These points would yield a slope of 4.2 ± 0.3.

4 SUMMARY AND CONCLUDING REMARKS

In this final paper of the series, we have investigated the correlation between photometric and global parameters of the sample of KKG. We find a clear increase in the scaleheight of the stellar disc as a function of maximum rotational velocity and dynamical mass. This is in general accordance with existing observations of the stellar kinematics; more massive spirals tend to contain discs that are more dynamically evolved and thicker. Remarkably, the disc flattening tends to increase towards lower face-on central surface brightness and larger dynamical mass-to-light ratio. This observation provides a link between the disc flattening and the Tully–Fisher relation, and predicts that for constant maximum rotational velocity the vertical stellar velocity dispersions of lower surface brightness discs are smaller.

We then further analysed the results obtained from the dynamical modelling of the stellar kinematics for a smaller sample of 15 galaxies. For a constant Q parameter, the data imply that the velocity anisotropy (σ_z/σ_R) decreases with an increasing disc contribution to the rotation curve ($v_{\rm disc}/v_{\rm max}$). If, on the other hand, σ_z/σ_R is constant among spirals, the data require a Q parameter that decreases with increasing $v_{\rm disc}/v_{\rm max}$. Several arguments suggest that $\sigma_z/\sigma_R = 0.6 \pm 0.1$ in intermediate- to late-type spirals.

At least 12 of the spirals in the present sample have submaximal discs. The average disc contribution for 13 spirals is $v_{\rm disc}/v_{\rm max} = 0.53 \pm 0.04$; only about 40 per cent of the mass within 2.2 disc scalelengths resides in the disc. Hence, the discs of intermediate- to late-type spiral galaxies probably inhabit dark matter haloes that dominate the mass fraction down to small galactocentric radii. We note, however, that very HSB spiral galaxies are underrepresented in our sample and the possibility remains that very HSB discs are maximal. The result is in agreement with earlier determinations based on stellar kinematics (B93), the absence of correlated scatter in the Tully–Fisher relation (Courteau & Rix 1999), spiral galaxy lensing (Trott & Webster 2002), and fluid dynamical modelling of normal spirals (Kranz et al. 2003). In addition, the average contribution for the six spirals with a boxy or peanut-shaped bulge is $v_{\rm disc}/v_{\rm max} = 0.56 \pm 0.09$, indistinguishable from the normal spirals. Since boxy and peanut-shaped bulges are probably associated with bars (Kuijken & Merrifield 1995; Bureau & Freeman 1999), this strongly suggests that the contribution of the disc to the rotation curve at $2.2\,h_R$ is independent of barredness. This is in good agreement with the recent high-resolution N-body simulations by Valenzuela & Klypin (2003). These point out that galaxies form bars even in the presence of strong haloes, and that the discs are submaximal at $2.2\,h_R$.

There is a relation between the stellar disc velocity dispersion and the galaxy maximum rotational velocity, confirming the work of B93. The deviations from the average σ versus $v_{\rm max}$ relation appear to correlate with disc flattening, face-on central surface brightness and dynamical mass-to-light ratio. Discs with a smaller radial stellar velocity dispersion tend to be more flattened, and have a lower surface brightness and a higher dynamical mass-to-light ratio. This is in agreement with the observed relation between disc flattening and dynamical mass-to-light ratio. The submaximal nature of galaxy discs and the scatter in the σ versus $v_{\rm max}$ relation are in good agreement with the simple collapse theory of disc galaxy formation (DSS97). The theory suggests that the σ versus $v_{\rm max}$ relation is the result of local stability: discs scatter about a linear σ versus $v_{\rm max}$ relation, with a slope corresponding to the average spin parameter of dark matter haloes and a scatter related to the spread in the spin parameter.

The Tully–Fisher (TF) relation is compared to the *HST* Key Project TF relation (Sakai et al. 2000). The luminosities of the edge-on spirals are based on an exponential vertical luminosity distribution and strictly apply to the old stellar population. The TF comparison shows that these luminosities are lower than the integrated luminosities by about 0.7 mag. Likely explanations are the missing luminosity from young stellar populations and residual dust

extinction at large distances from the plane. The dynamical stellar disc mass TF relation is compared to the maximum-disc scaled stellar mass TF relation of the Ursa Major cluster (BJ01). The dynamical disc mass TF is offset from the maximum-disc scaled stellar mass TF relation by -0.3 dex in mass. The offset is mirrored in the baryonic TF relations and is naturally explained if the discs of the Ursa Major cluster spirals are submaximal.

The submaximal nature of galaxy discs, the σ versus $v_{\rm max}$ relation and the three-parameter relation between central surface brightness, dynamical mass-to-light ratio and disc flattening are also in good agreement with the simple collapse theory of the formation of disc galaxies in virialized dark matter haloes (DSS97; Mo et al. 1998). In this picture, discs make a range of contributions to the maximum rotation, from strongly submaximal in haloes of higher-than-average spin angular momentum towards less submaximal in haloes of low spin angular momentum. The scatter in the σ versus $v_{\rm max}$ relation results from the spread in halo spin parameters and the stability parameter Q. According to the collapse model, the observed trend that discs with a lower stellar velocity dispersion tend to be flatter, of lower central surface brightness and of higher dynamical mass-to-light ratio corresponds to the notion that more extended discs arise from higher spin angular momentum dark haloes.

ACKNOWLEDGMENTS

We would like to thank Erwin de Blok and Rob Swaters for valuable comments that helped to improve this paper.

REFERENCES

Athanassoula E., Sellwood J. A., 1986, MNRAS, 221, 213
Athanassoula E., Bosma A., Papaioannou S., 1987, A&A, 179, 23
Begeman K. G., 1987, PhD thesis, Univ. Groningen
Bell E. F., de Jong R. S., 2000, MNRAS, 312, 497
Bell E. F., de Jong R. S., 2001, ApJ, 550, 212 (BJ01)
Bizyaev D., Mitronova S., 2002, A&A, 389, 795
Boissier S., Prantzos N., Boselli A., Gavazzi G., 2003, MNRAS, 346, 1215
Bosma A., 1978, PhD thesis, Univ. Groningen
Bosma A., 1999, in Merritt D., Sellwood J. A., Valluri M., eds, ASP Conf. Ser. Vol. 182, Galaxy Dynamics. Astron. Soc. Pac., San Francisco, p. 339
Bottema R., 1993, A&A, 275, 16 (B93)
Bottema R., 1995, PhD thesis, Univ. Groningen
Bottema R., 1997, A&A, 328, 517
Bottema R., 1999, A&A, 348, 77
Bottema R., 2003, MNRAS, 344, 358
Broeils A. H., Courteau S., 1997, in Persic M., Salucci P., eds, ASP Conf. Ser. Vol. 117, Dark and Visible Matter in Galaxies and Cosmological Implications. Astron. Soc. Pac., San Francisco, p. 74
Bullock J. S., Dekel A., Kolatt T. S., Kravtsov A. V., Klypin A. A., Porciani C., Primack J. R., 2001a, ApJ, 555, 240
Bullock J. S., Kolatt T. S., Sigad Y., Somerville R. S., Kravtsov A. V., Klypin A. A., Primack J. R., Dekel A., 2001b, MNRAS, 321, 559
Bureau M., Freeman K. C., 1999, AJ, 118, 126
Buta R., Crocker D. A., Elmegreen B. G., eds, 1996, ASP Conf. Ser. Vol. 91, IAU Colloq. 157, Barred Galaxies. Astron. Soc. Pac., San Francisco
Courteau S., Rix H.-W., 1999, ApJ, 513, 561
Courteau S., Andersen D. R., Bershady M. A., MacArthur L. A., Rix H.-W., 2003, ApJ, 594, 208
Dalcanton J. J., Spergel D. N., Summers F. J., 1997, ApJ, 482, 659 (DSS97)
de Blok W. J. G., McGaugh S. S., van der Hulst J. M., 1996, MNRAS, 283, 18
de Grijs R., 1997, PhD thesis, Univ. Groningen (http://www.ub.rug.nl/eldoc/dis/science/r.de.grijs)
de Grijs R., 1998, MNRAS, 299, 595
de Grijs R., Peletier R. F., van der Kruit P. C., 1997, A&A, 327, 966
Dehnen W., Binney J. J., 1998, MNRAS, 298, 387
de Jong R. S., 1996a, A&A, 313, 45
de Jong R. S., 1996b, A&A, 313, 377
de Jong R. S., Lacey C., 2000, ApJ, 545, 781
Englmaier P., Gerhard O., 1999, MNRAS, 304, 512
Fall S. M., Efstathiou G., 1980, MNRAS, 193, 189
Freeman K. C., 1970, ApJ, 160, 811
Freeman K. C., 1992, in Thuan T. X., Bakowski C., Van J. T. T., eds, Physics of Nearby Galaxies, Nature or Nurture. Editions Frontières, Gif-sur-Yvette, p. 201
Freeman K. C., 2002, in Athanassoula E., Bosma A., eds, ASP Conf. Ser. Vol. 275, Disks of Galaxies: Kinematics, Dynamics and Perturbations. Astron. Soc. Pac., San Francisco, p. 3
Fuchs B., 1999, in Merritt D., Sellwood J. A., Valluri M., eds, ASP Conf. Ser. Vol. 182, Galaxy Dynamics. Astron. Soc. Pac., San Francisco, p. 365
Gerssen J., Kuijken K., Merrifield M. R., 1997, MNRAS, 288, 618
Gerssen J., Kuijken K., Merrifield M. R., 2000, MNRAS, 317, 545
Graham A. W., 2002, MNRAS, 334, 721
Griv E., Rosenstein B., Gedalin M., Eichler D., 1999, A&A, 347, 821
Gunn J. E., 1982, in Longair M. S., Coyne G. V., Bruck H. A., eds, Astrophysical Cosmology. Pontifica Academia Scientiarum, Vatican City, p. 233
Hohl F., 1971, ApJ, 168, 343
Howk J. C., Savage B. D., 1999, AJ, 117, 2077
Isobe T., Feigelson E. D., Akritas M. G., Babu G. J., 1990, ApJ, 364, 104
Jenkins A., Binney J., 1990, MNRAS, 245, 305
Jones T. J., Ashley M., Hyland A. R., Ruelas-Mayorga A., 1981, MNRAS, 197, 413
Kalnajs A. J., 1983, in Athanassoula E., ed., Proc. IAU Symp. 100, Internal Kinematics of Galaxies. Reidel, Dordrecht, p. 87
Karachentsev I. D., Karachentseva V. E., Kudrya Y. N., Sharina M. E., Parnovsky S. L., 1999, Bull. Special Astrophys. Obs., 47, 5
Kent S. M., 1986, AJ, 91, 1301
Kranz T., Slyz A., Rix H.-W., 2003, ApJ, 586, 143
Kregel M., 2003, PhD thesis, Univ. Groningen (http://www.ub.rug.nl/eldoc/dis/science/m.kregel)
Kregel M., van der Kruit P. C., 2004, MNRAS, 352, 787 (Paper III)
Kregel M., van der Kruit P. C., 2005, MNRAS, in press (doi:10.1111/j.1365-2966.2005.08811.x) (Paper IV, this issue)
Kregel M., van der Kruit P. C., de Grijs R., 2002, MNRAS, 334, 646 (KKG)
Kregel M., van der Kruit P. C., Freeman K. C., 2004a, MNRAS, 351, 1247 (Paper I)
Kregel M., van der Kruit P. C., de Blok W. J. G., 2004b, MNRAS, 352, 768 (Paper II)
Kroupa P., 2002, Sci, 295(5552), 82
Kudrya Y. N., Karachentsev I. D., Karachentseva V. E. Parnovskii S. L., 1994, Astron. Lett., 20, 8
Kuijken K., Merrifield M. R., 1995, ApJ, 443, L13
Lewis J. R., Freeman K. C., 1989, AJ, 97, 139
McGaugh S. S., de Blok W. J. G., 1998, ApJ, 499, 41
McGaugh S. S., Schombert J. M., Bothun G. D., de Blok W. J. G., 2000, ApJ, 533, 99
Maller A. H., Simard L., Guhathakurta P., Guhathakurta P., Hjorth J., Jaunsen A. O., Flores R. A., Primack J. R., 2000, ApJ, 533, 194
Mignard F., 2000, A&A, 354, 522
Mihos J. C., McGaugh S. S., de Blok W. J. G., 1997, ApJ, 477, 79
Mo H. J., Mao S., White S. D. M., 1998, MNRAS, 295, 319
Narayan C. A., Jog C. J., 2002, A&A, 390, L35
Palunas P., Williams T. B., 2000, AJ, 120, 2884
Peebles P. J. E., 1969, ApJ, 155, 393
Pignatelli E. et al., 2001, MNRAS, 323, 188
Pohlen M., Dettmar R.-J., Lütticke R., 2000, A&A, 357, 1
Portinari L., Sommer-Larsen J., Tantalo R., 2004, MNRAS, 347, 691P
Rhoads J. E., 1998, AJ, 115, 472
Sackett P. D., 1997, ApJ, 483, 103
Sakai S., Mould J. R., Hughes S. M. G., Huchra J. P., 2000, ApJ, 529, 698

Sellwood J. A., Carlberg R. G., 1984, ApJ, 282, 61
Shapiro K. L., Gerssen J., van der Marel R. P., 2003, AJ, 126, 2707
Swaters R. A., 1999, PhD thesis, Univ. Groningen (http://www.ub.rug.nl/eldoc/dis/science/r.a.swaters)
Toomre A., 1964, ApJ, 139, 1217
Toomre A., 1981, in Fall S. M., Lynden-Bell D., eds, The Structure and Evolution of Normal Galaxies. Cambridge Univ. Press, Cambridge, p. 111
Trott C. M., Webster R. L., 2002, MNRAS, 334, 621
Tully R. B., Fouque P., 1985, ApJS, 58, 67
Tully R. B., Pierce M. J., Huang J. S., Saunders W., Verheijen M. A. W., Witchalls P. L., 1998, AJ, 115, 2264
Valenzuela O., Klypin A., 2003, MNRAS, 345, 406
van Albada T. S., Bahcall J. N., Begeman K., Sancisi R., 1985, ApJ, 295, 305
van der Kruit P. C., 1988, A&A, 192, 117
van der Kruit P. C., 1990, in Gilmore G., King I. R., van der Kruit P. C., eds, The Milky Way as a Galaxy. University Science Books, Mill Valley, CA, p. 198
van der Kruit P. C., 1995, in van der Kruit P. C., Gilmore G., eds, Proc. IAU Symp. 164, Stellar Populations. Kluwer, Dordrecht, p. 227
van der Kruit P. C., 2001a, in Funes J. G., Corsini E. M., eds, ASP Conf. Ser. Vol. 230, Galaxy Disks and Disk Galaxies. Astron. Soc. Pac., San Francisco, p. 119
van der Kruit P. C., 2001b, in Da Costa G. S., Jerjen H., eds, ASP Conf. Ser. Vol. 273, The Dynamics, Structure and History of Galaxies. Astron. Soc. Pac., San Francisco, p. 7
van der Kruit P. C., de Grijs R., 1999, A&A, 352, 129
van der Kruit P. C., Freeman K. C., 1984, ApJ, 278, 81
van der Kruit P. C., Freeman K. C., 1986, ApJ, 303, 556
van der Kruit P. C., Searle L., 1981, A&A, 95, 116
van der Kruit P. C., Searle L., 1982, A&A, 110, 61
van der Kruit P. C., Jiménez-Vicente J., Kregel M., Freeman K. C., 2001, A&A, 379, 374
Verheijen M. A. W., 1997, PhD thesis, Univ. Groningen (http://www.ub.rug.nl/eldoc/dis/science/m.a.w.verheijen)
Verheijen M. A. W., 2001, ApJ, 563, 694
Wang B., Silk J., 1994, ApJ, 427, 759
Warren M. S., Quinn P. J., Salmon J. K., Zurek W. H., 1992, ApJ, 399, 405
Weiner B. J., Sellwood J. A., Williams T. B., 2001, ApJ, 546, 931
Worthey G., 1994, ApJS, 95, 107
Xilouris E. M., Byun Y. I., Kylafis N. D., Paleologou E. V., Papamastorakis J., 1999, A&A, 344, 868
Zasov A. V., Bizyaev D. V., Makarov D. I., Tyurina N. V., 2002, Astron. Lett., 28, 527
Zavala J., Avila-Reese V., Hernández-Toledo H., Firmani C., 2003, A&A, 412, 633
Zwaan M. A., van der Hulst J. M., de Blok W. J. G., McGaugh S. S., 1995, MNRAS, 273, L35

This paper has been typeset from a TEX/LATEX file prepared by the author.